

1 Spatial and temporal dynamics of suspended sediment concentrations in coastal waters of South
2 China Sea, off Sarawak, Borneo: Ocean colour remote sensing observations and analysis

3 Jenny Choo¹, Nagur Cherukuru², Eric Lehmann², Matt Paget², Aazani Mujahid³, Patrick Martin⁴, Moritz Müller¹

4 ¹Swinburne University of Technology, Faculty of Engineering, Computing and Science, Jalan Simpang Tiga, 93350 Kuching,
5 Sarawak, Malaysia.

6 ²Commonwealth Scientific and Industrial Research Organization (CSIRO), Canberra ACT 2601, Australia.

7 ³Faculty of Resource Science & Technology, University Malaysia Sarawak, Kota Samarahan 94300, Sarawak, Malaysia.

8 ⁴Asian School of the Environment, Nanyang Technological University, 639798, Singapore.

9
10 Correspondence to: Jenny Choo (JChoo@swinburne.edu.my/jccy89@gmail.com)

11
12 Abstract

13 High-quality ocean colour observations are increasingly accessible to support various monitoring and
14 research activities for water quality measurements. In this paper, we present a newly developed
15 regional total suspended solids (TSS) empirical model using MODIS-Aqua's Rrs(530) and Rrs(666)
16 reflectance bands to investigate the spatial and temporal variation of TSS dynamics along the
17 southwest coast of Sarawak, Borneo, [with the application of the Open Data Cube \(ODC\) platform](#). The
18 performance of this TSS retrieval model was evaluated using error metrics (bias = 1.0, MAE = 1.47, and
19 RMSE = 0.22 in mg/L) with a log10 transformation prior to calculation, as well as a k-fold cross
20 validation technique. The temporally averaged map of TSS distribution, using daily MODIS-Aqua
21 satellite datasets from 2003 until 2019, revealed large TSS plumes detected particularly in the Lupar
22 and Rajang coastal areas on a yearly basis. The average TSS concentration in these coastal waters was
23 in the range of 15 – 20 mg/L. Moreover, the spatial map of TSS coefficient of variation (CV) indicated
24 strong TSS variability (approximately 90 %) in the Samunsam-Sematan coastal areas, which could
25 potentially impact nearby coral reef habitats in this region. Study of ~~the~~ temporal TSS variation
26 provides further evidence that monsoonal patterns drive the TSS release in these tropical water
27 systems, with distinct and widespread TSS plume variations observed between the northeast and
28 southwest monsoon periods. A map of relative TSS distribution anomalies revealed strong spatial TSS
29 variations in the Samunsam-Sematan coastal areas, while 2010 recorded a major increase
30 (approximately 100 %) and widespread TSS distribution with respect to the long-term mean.
31 Furthermore, study of ~~the~~ contribution of river discharge to the TSS distribution showed a weak
32 correlation across time at both the Lupar and Rajang river mouth points. The variability of TSS
33 distribution across coastal river points was studied by investigating the variation of TSS pixels at three
34 transect points, stretching from the river mouth into territorial and open water zones, for eight main
35 rivers. ~~The r~~Results showed a progressively decreasing pattern of nearly 50 % in relation to the
36 distance from shore, with exceptions in the northeast regions of the study area. Essentially, our
37 findings demonstrate that the TSS levels at the southwest coast of Sarawak are within local water
38 quality standards, promoting various marine and socio-economic activities. This study presents the
39 first observation of TSS distributions at Sarawak coastal systems with the application of remote
40 sensing technologies, to enhance coastal sediment management strategies for the sustainable use of
41 coastal waters and their resources.

42 Keywords: total suspended solids, band-ratio, monsoon, river discharge, Open Data Cube

43

44

45

46 1.0 Introduction

47 Total Suspended Solids (TSS) play an important role in the aquatic ecosystem as one of the primary
48 water quality indicators of coastal and riverine systems (Alcântara et al., 2016; Cao et al., 2018; Chen
49 et al., 2015a; González Vilas et al., 2011; Mao et al., 2012). For example, elevated concentrations of
50 TSS in water have an adverse impact on fisheries and biodiversity of the aquatic ecosystem (Bilotta
51 and Brazier, 2008; Chapman et al., 2017; Henley et al., 2000; Wilber and Clarke, 2001). Understanding
52 the impacts of varying water quality in relation to TSS status has been one of the primary concerns
53 with respect to a country's growing Blue Economy status and sustainable management of aquatic
54 resources (Lee et al., 2020a; Sandifer et al., 2021; World Bank and United Nations Department of
55 Economic and Social Affairs (UNDESA), 2017). With about 40 % of the world's population living within
56 100 km of coastal areas (United Nations, 2017), and with more than 80 % of the population in Malaysia
57 living within 50 km of the coast (Praveena et al., 2012), water quality monitoring and management
58 efforts are important at both regional and global scale.

59 Studying TSS distribution can provide insights into the connections between land and ocean
60 ecosystems (Howarth, 2008; Lemley et al., 2019; Lu et al., 2018). For instance, TSS dynamics allow us
61 to understand the impacts of sediment transport and sediment plumes, particularly in areas
62 experiencing large-scale deforestation, land conversion and damming of rivers (Chen et al., 2007;
63 Espinoza Villar et al., 2013). Sarawak, Malaysian Borneo, experienced significant land use and land
64 cover change activities over the past four decades, with widespread land conversion and deforestation
65 for developments and large-scale plantation activities (Gaveau et al., 2016), as well as building of
66 major road infrastructures, such as the Pan-Borneo highway, and hydroelectric dams (Alamgir et al.,
67 2020). As a result, river and coastal systems may potentially drive large TSS loads into downstream
68 systems and into the marine and open ocean waters.

69 Situated at the southern part of the South China Sea, the region of Sarawak, Malaysian
70 Borneo, has a coastline of about 1035 km where mangrove forests are dominant (Long, 2014). The

71 coastal regions of Sarawak are rich with marine coastal biodiversity and coral reefs, which can be
72 found at the northeast and southwest part of Sarawak (Praveena et al., 2012). While the coasts of
73 Sarawak provide important socio-economic values to the local communities (Lee et al., 2020b), these
74 coastal areas are potentially facing water quality degradation from TSS riverine outputs in response
75 to land use and land cover change activities.

76 TSS concentrations are commonly measured through conventional laboratory-based methods
77 to quantify TSS concentrations by field collection of water samples (Ling et al., 2016; Mohammad Razi
78 et al., 2021; Soo et al., 2017; Soum et al., 2021; Tromboni et al., 2021; Zhang et al., 2013). Currently,
79 real-time high-frequency TSS observations using modern optical and bio-sensor systems are also
80 possible (Bhardwaj et al., 2015; Horsburgh et al., 2010). These sensors can be generally found onboard
81 ship and buoy-based observation platforms. Yet, it remains a challenge to quantify TSS concentrations
82 of large spatial coverage and high temporal frequency with these approaches.

83 Ocean colour remote sensing technologies represent an increasingly accessible and powerful
84 tool to provide a synoptic view for short or long-term water quality studies at high temporal and spatial
85 resolutions (Cherukuru et al., 2016a; Slonecker et al., 2016; Swain and Sahoo, 2017; Wang et al., 2017;
86 Werdell et al., 2018). Remote sensing can help overcome several constraints of conventional intensive
87 field campaigns such as: (i) costly field campaigns from boat rentals or cruise; (ii) time-consuming and
88 inadequate manpower; and most importantly for this study, (iii) limited spatial and temporal field
89 coverage. NASA's Moderate Resolution Imaging Spectroradiometer (MODIS)-Aqua
90 (<https://modis.gsfc.nasa.gov/about/>) has a distinctive advantage with its daily revisit time, a spatial
91 resolution of 250 – 1000 m, and a large collection of ocean colour data since 2002. Other sensors
92 offering ocean colour measurement capabilities include Landsat-8, which, in comparison with MODIS-
93 Aqua, has a 16-day revisit time and high spatial resolution of 30 m. Additionally, Sentinel 2-MSI and
94 Sentinel 3-OLCI missions provide global coverage of high resolution (10 – 20 m) of ocean and land
95 observation services, with revisit time of 10-day and 2-day, respectively (European Space Agency,

96 2022a, 2022b). Despite Landsat 8 and Sentinel-2's powerful ability in capturing higher resolution
97 images, the longer revisit interval may not be suitable for characterizing and studying water bodies
98 with high dynamics of various water constituents. While Sentinel 3-OLCI enhances in a shorter revisit
99 time, this mission has a relatively smaller collection of ocean data stored, with the mission launched
100 in 2016, in comparison to the MODIS-Aqua data collection.

101 Several MODIS-derived models have been developed for TSS retrievals (Chen et al., 2015b;
102 Espinoza Villar et al., 2013; Jiang and Liu, 2011; Kim et al., 2017; Zhang et al., 2010b), including
103 empirical, semi-analytical and machine-learning approaches (Balasubramanian et al., 2020; Jiang et
104 al., 2021). However, the performance of these models proved to be unsatisfactory~~less satisfactory~~,
105 with recorded low r^2 and high bias and mean absolute error (MAE) values when tested with in situ TSS
106 datasets (Supplementary Materials, Table S1). Generally, water types are categorised as clear, as well
107 as coloured dissolved organic matter (CDOM) and sediment-rich waters, due to the presence of
108 various optical water constituents in these water columns (Balasubramanian et al., 2020). While these
109 global TSS remote sensing models address the need to improve TSS retrievals and to monitor global
110 TSS trends in various water class types, they tend to underperform in more localised and regional
111 studies (Mao et al., 2012; Ondrusek et al., 2012). The coastal waters of Borneo are well-mixed
112 throughout the year and enriched with suspended material and dissolved organic matter (Müller et
113 al., 2016). Various water quality studies of the river systems have been actively carried out to assess
114 the dynamics of numerous water quality constituents in response to human activities, with TSS
115 concentrations being one of the primary environmental concerns in this region (Ling et al., 2016;
116 Müller-dum et al., 2019; Tawan et al., 2020). Although studies on the water quality of coastal systems
117 in Borneo have gradually gained much attention (Cherukuru et al., 2021; Limcih et al., 2010; Martin et
118 al., 2018; Soo et al., 2017), there is still much knowledge to gain on the understanding of how coastal
119 waters in the region have been impacted by TSS loadings and transport over large spatial and temporal
120 scales. ▲

Formatted: Not Highlight

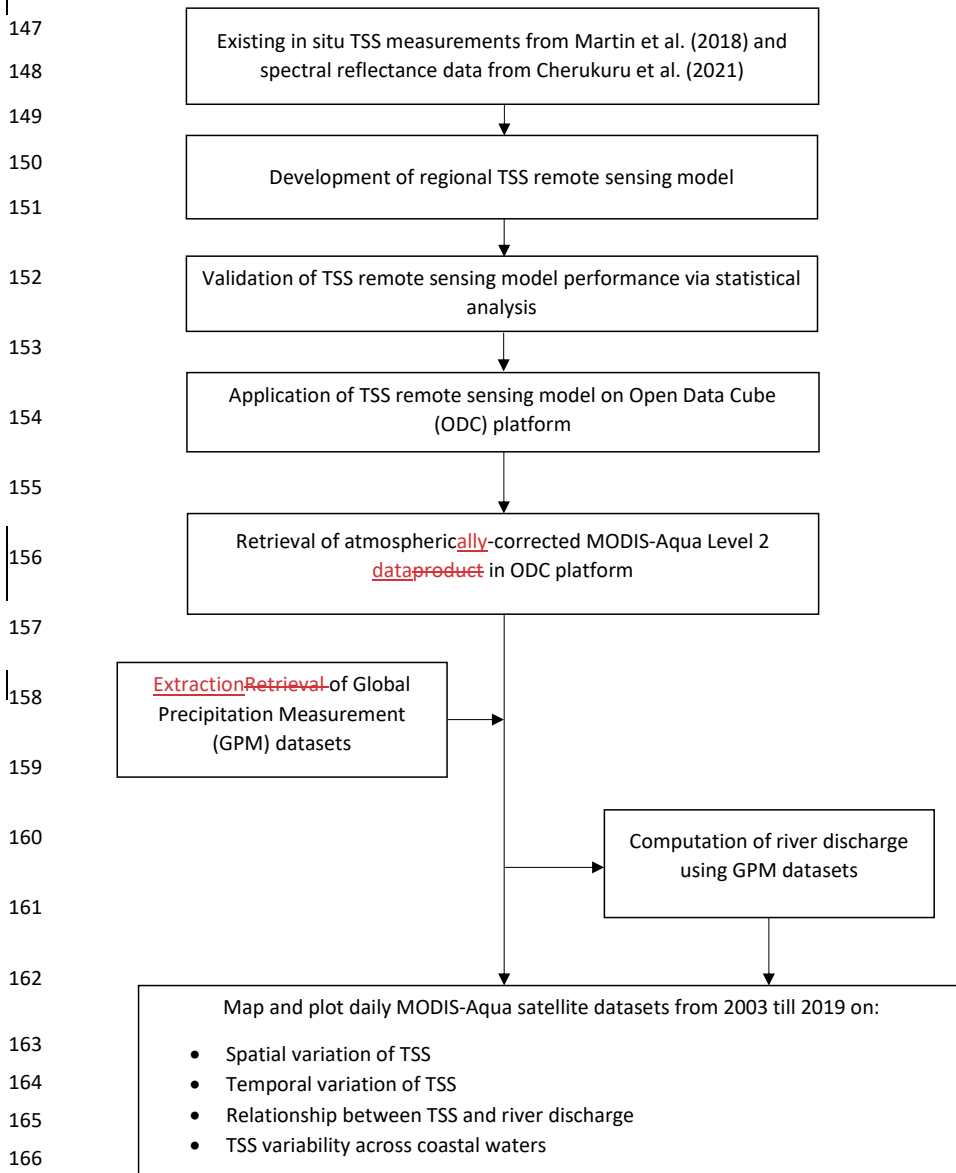
121 Here, in this paper, we present a new regional empirical TSS remote sensing model. While
122 various remote sensing models have their own unique computational strengths, this study
123 demonstrates the reliability of a band ratio TSS model ~~when to be~~ applied ~~in~~ within optically complex
124 waters. With the ongoing efforts to address and minimize water quality degradation in coastal
125 systems, as outlined in the United Nation's Sustainability Development Goals no. 14, our study aims
126 to apply the new empirical regional TSS remote sensing model to: (a) investigate the spatial and
127 temporal variability in TSS, (b) identify hotspots of TSS distribution in the coastal waters of Sarawak,
128 Malaysian Borneo, using a long time series of MODIS-Aqua data from year 2003 until 2019, and (c)
129 study the varying monsoonal and river discharge patterns in relation to TSS distribution at the river
130 mouths located within the study case area.~~With the growing accessibility of freely available satellite~~
131 ~~datasets, the application of Open Data Cube (ODC) platform provides an advanced tool to access~~
132 ~~scalable spatial imageries datasets and process time-series satellite data for earth observation studies~~
133 ~~(Open Data Cube, 2021). As such, this study implements the application of ODC platform which is~~
134 ~~further demonstrated in this study.~~

135
136
137
138
139
140
141
142
143

Formatted: Indent: First line: 0 cm

144 2.0 Methodologies

145 The figure below summarizes the processes carried out in this study. Spatial and temporal variation
146 of TSS distribution was mapped using an atmospherically-corrected MODIS-Aqua Level 2 product.



167 Fig. 1: Flowchart summarizing the processes of developing a regional TSS remote sensing model and applying it to analyse
168 the spatial and temporal variation of TSS over the study region, using MODIS-Aqua data from year 2003 until 2019. Long-
169 term MODIS-Aqua datasets were analysed and mapped on an Open Data Cube (ODC) platform with implementation of robust
170 Python libraries and packages.

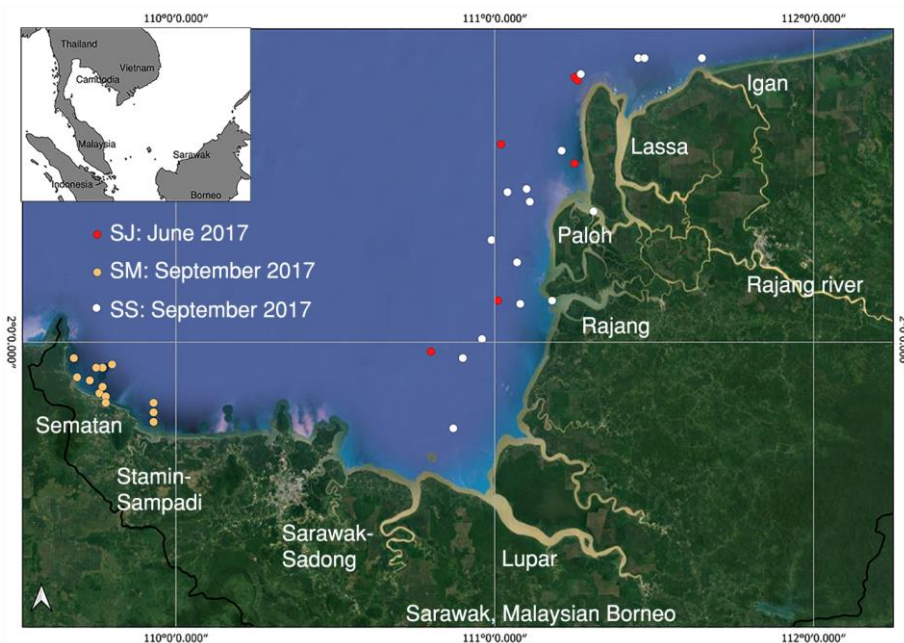
171

172 2.1 Area of study

173 Our study focuses on the southwestern coast of Sarawak (between 1.9° N, 109.65° E and 2.8° N, 111.5°
174 E) in Malaysia, which sits at the northwest part of the Borneo Island. Generally, the island of Borneo
175 (between 3.01° S, 112.18° E and 6.45° N, 117.04° E) contains rich tropical rainforests and biodiversity
176 on the lands of Sarawak and Sabah (Malaysia), Brunei, and Indonesia. Typically, Sarawak is a tropical
177 climate region, recording an average ambient temperature of 27.8 °C (variation of 1.8 °C) throughout
178 the year. It records high precipitation with an average of 4116.7 mm/yr in Kuching (1.5535° N,
179 110.3593° E), the capital city of Sarawak. Yearly, it experiences both a dry and wet season, which is
180 influenced by: (i) the southwestern monsoon (May to September) and (ii) the northeastern monsoon
181 (November to March). Rivers in Sarawak are connected to the South China Sea and flow through
182 various plantation types, such as ~~palm oil~~~~oil-palm~~, rubber and sago (Davies et al., 2010).

183 In this study, the southwestern part of Sarawak's coastal regions (Fig. 2), (between 1.9° N, 109.65° E
184 and 2.8° N, 111.5° E) was studied, which comprises several major rivers (e.g. Lupar, Sebuyau,
185 Sematan), as well as the Rajang River, the longest river in Malaysia. Rajang river basin consists of a ~~tidally~~~~influenced~~
186 river channel which splits into a northwest (Igan, Lassa and Paloh) and a southwest
187 (Rajang, Belawai) Rajang river delta (Staub et al., 2000). The Rajang river basin drains a dominant area
188 (>50,000km²) of sedimentary rocks (Milliman and Farnsworth, 2013; Staub et al., 2000) extending
189 from Belaga to Sibu, with major peatland areas converted into ~~palm oil~~~~oil-palm~~ plantations (Gaveau
190 et al., 2016) as its river flows into the South China Sea (Milliman and Farnsworth, 2013). Major
191 settlements along the Rajang river comprise of Kapit and Kanowit town areas, as well as Sibu city, with
192 a total population size of about 388,000 inhabitants (Department of Statistics, 2020). Lupar and
193 Saribas rivers, respectively, comprise a catchment area size of approximately 6500 and 1900 km²
194 (Lehner et al., 2006). Situated at the southwest side of the Rajang catchment, Lupar and Saribas rivers

195 surround the Maludam National Park, which is Sarawak's remaining biggest single patch of peat
196 swamp forest (Sarawak Forestry Corporation, 2022). Adjacent to Lupar river mouth is the Sadong river,
197 with an approximate catchment area size of 3500 km² (Kuok et al., 2018). Sadong river ~~is runs~~ about
198 150 km long and flows through palm oil oil-palm plantations (Staub and Esterle, 1993). These river
199 systems are associated with increasing land use activities and land cover changes in this region, which
200 essentially transport and connect various biogeochemical water components to the coastal systems
201 of Sarawak.



202
203 Fig. 2: Map of the study area (© Google Maps), located in the southwestern part of Sarawak, Malaysia (inset). Indicators
204 show the location of sampling sites used during field expeditions carried out in June and September 2017.

205 2.2 In situ TSS measurements

206 TSS measurements were taken from Martin et al. (2018). A total of 35 coastal sites were studied and
207 are denoted SJ, SS, and SM (see: Table 1 & Fig. 2). These water samples were collected in the month
208 of June (SJ region) and September (SS and SM regions) in 2017. Water samples were filtered, and

209 filters were dried and ashed prior to ~~the~~ weighing process. Full details of ~~the~~ water sampling and TSS
210 analysis ~~are~~ available in Martin et al. (2018).

211 2.3 Development, calibration and validation of TSS model

212 In situ remote sensing reflectance spectral data, $Rrs(\lambda)$, along with 35 measured TSS values, were used
213 to develop a new remote sensing TSS empirical model for MODIS-Aqua for this case study. Field
214 measurements of SM, SJ & SS datasets, as shown in Table 1, were used to calibrate the MODIS-Aqua
215 TSS remote sensing model.

216 For the in situ remote sensing reflectance, $Rrs(\lambda)$ readings, a TriOS-RAMSES spectral imaging
217 radiometer was used to measure downwelling irradiance, $Ed(\lambda)$, and upwelling radiance, $Lu(\lambda)$, with
218 measurement protocols from Mueller et al. (2002). These measurements were recorded under stable
219 sky and sea conditions during the day (10AM to 4PM) with high solar elevation angles.

220 Measurements of reflectance, $Rrs(\lambda)$, were recorded concurrently with the collection of water samples
221 (as described in Section 2.2) and were recorded at wavelength ranging from 280 to 950 nm, which
222 covers the spectrum of ultraviolet, visible and ~~near-infrared bands visible/ultraviolet light~~. These
223 measurements were recorded on a float to capture $Lu(0-, \lambda)$ and $Ed(0+, \lambda)$, where 0- and 0+ refer to
224 below-surface and above-surface, respectively.

225 Remote sensing reflectance, $Rrs(\lambda)$, was computed as follows with reference to Mueller et al. (2002):

$$Rrs(\lambda, 0+) = \frac{1 - p}{n^2} \times \frac{Lu(0-, \lambda)}{Ed(0+, \lambda)} \quad (1)$$

226 where $p = 0.021$ refers to the Fresnel reflectance and $n = 1.34$ is the refractive index of water. Full
227 details of this methodology can be found at Cherukuru et al. (2021).

228 2.3.1 Calibration of empirical model and application to MODIS-Aqua

229 With the intention to apply a regional TSS remote sensing model to MODIS-Aqua ~~dataproduet~~, a total
230 of 35 ~~in situ spectral data of~~ different ~~datasets of~~ TSS concentrations ~~datasets were collected in coastal~~

231 conditions (salinity > 15 PSU) and convolved to generate MODIS-Aqua data, which were collected in
232 coastal conditions (salinity > 15 PSU), were convolved with MODIS-Aqua spectral response function
233 values (Pahlevan et al., 2012) at each centre wavelength of individual band channels (NASA official,
234 2022). MODIS-Aqua offers visible bands of violet/blue (412, 443, 469, and 488 nm), green (531, 547,
235 and 555 nm), red (645, 667, and 678 nm) and near-infrared wavelengths (748, 859 and 869 nm) for
236 remote sensing of coastal waters (NASA official, 2022). The in situ spectra data were resampled to
237 MODIS-Aqua's central spectral bands based on the aforementioned information. Measurements of in
238 situ spectral data enhance the understanding of bio-optical water characteristics of a localised region,
239 and increase the sensitivity of radiometric measurements without atmospheric interferences, while
240 subject to the radiometer's calibration condition (Brezonik et al., 2015; Cui et al., 2010; Dorji and
241 Fearn, 2017; Slonecker et al., 2016).

242 In this study, retrieval of water constituents was established using spectral band ratio combinations
243 which have proven to be a straightforward, yet reliable method for estimating water constituents in
244 optically turbid waters (Ahn and Shanmugam, 2007; Cao et al., 2018; Lavigne et al., 2021; Morel and
245 Gentili, 2009; Neil et al., 2019; Siswanto et al., 2011). Band ratio models help to offset signal noise,
246 such as the effects of the atmosphere and irradiance of spectral reflectance to a certain degree
247 (Cherukuru et al., 2016b; Ha et al., 2017; Hu et al., 2012; Liu et al., 2019).

248 A variety of models using single bands, as well as a combination of MODIS-Aqua's Blue, Green & Red
249 bands (412nm, 440nm, 488nm, 532nm, 555nm & 660nm) were calibrated using field measurements
250 as the dependent variable. The calibration process was tested out using various model functions,
251 including linear, power, exponential, and logarithmic functions. The best empirical TSS retrieval model
252 was fitted by means of a regression between the in situ TSS data and in situ radiometer values, and
253 can be expressed as follows:

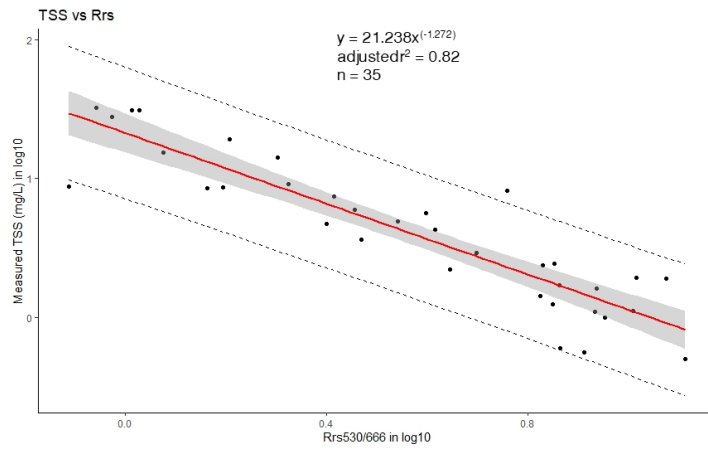
$$254 \quad \text{TSS} = 21.238[\text{Rrs}(530)/\text{Rrs}(666)]^{-1.272} \quad (2)$$

255 This power function model resulted in a coefficient of determination (R^2) of 0.82 (Fig. 3).

256 Table 1: Summary statistics of TSS values collected at areas SJ, SS, and SM located within coastal regions in this study, with a
 257 total of 35 datasets recorded.

Coastal Area	Minimum	Maximum	Mean	S.D.	C.V.	n
SJ	1.1	19.24	6.89	6.62	96.09	6
SS	0.56	32.1	12.50	11.43	91.45	16
SM	0.5	8.14	2.59	2.70	104.53	13

258



259

260 Fig. 3: Empirical relationship of TSS retrieval between in situ Rrs(530)/Rrs(666) bands ratio and measured TSS
 261 concentration (mg/L), as established via a power law function. Upper and lower dashed lines indicate the 95 % prediction
 262 interval of the regression.

263 2.3.2 Performance assessment and validation of MODIS-Aqua empirical model

264 An assessment of the performance error of the newly developed TSS model was carried out as per
 265 Seegers et al. (2018)'s recommendation for interpreting ocean colour models. These performance
 266 metrics used here include the bias, Mean Absolute Error (MAE), Root Mean Squared Error (RMSE),
 267 coefficient of variation (CV), as well as the coefficient determination, r^2 , based on the following
 268 calculations:

$$269 \text{ Bias} = 10^{\left[\frac{\sum_{i=1}^n \log_{10}(Mi) - \log_{10}(Oi)}{n} \right]} \quad (3)$$

$$270 \text{ MAE} = 10^{\left[\frac{\sum_{i=0}^n | \log_{10}(Mi) - \log_{10}(Oi) |}{n} \right]} \quad (4)$$

271
$$\text{RMSE} = \sqrt{\frac{\sum_{i=1}^n (\log_{10}(M_i) - \log_{10}(O_i))^2}{n}} \quad (5)$$

272
$$\text{CV} = \frac{\sigma}{\mu} \times 100\% \quad (6)$$

273 where M represents the modelled TSS values, n is the number of samples, and O represents the
 274 observed TSS measurements, while σ refers to standard deviation and μ represents the mean value.

275 Equations (3), (4) and (5) use a log10-transform of the data as the range of TSS values can span several
 276 orders of magnitude. As such, an application of the log-transformation prior to error metric calculation
 277 allows us to account for uncertainties that are proportional to the concentration values
 278 (Balasubramanian et al., 2020; Seegers et al., 2018).

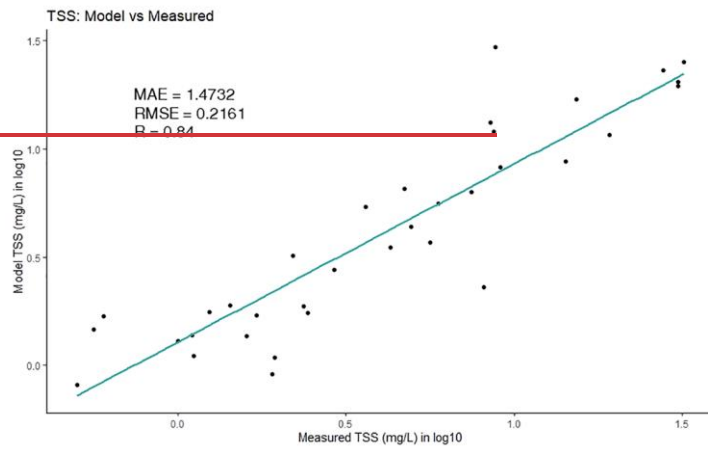
279 Table 2: Calibration and accuracy assessment of the newly derived MODIS-Aqua models in this study for TSS estimations
 280 tested using various model functions. Calculation for bias, MAE and RMSE use a log-transformation of the data prior to
 281 calculation of error metric measurements, as adapted from Seegers et al. (2018) and Balasubramanian et al. (2020). Band
 282 ratio Rrs(530)/Rrs(666) is established as function x. The pPower function model is selected based on low performance metric
 283 values.

Model	Function	Bias	MAE	RMSE	CV (%)	R
Power	TSS = 21.238x ^{-1.272}	0.9999	1.4732	0.2161	4.74	0.84
Linear	TSS = -1.8193x + 16.928	1.4463	1.8549	6.7174	20.699	0.6854
Exponential	TSS = 17.784e ^{-0.296x}	1.0791	1.4906	6.3088	3.8920	0.8154
Logarithmic	-8.872ln(x)+19.383	1.1336	1.6177	5.3735	-17.056	0.8128

284

285

286



287

288 Fig. 4: Scatterplot of modelled TSS values derived from the proposed model and measured TSS values (mg/L).

289 An evaluation of the model was performed using a k-fold cross validation technique (Refaeilzadeh et
 290 al., 2020) given the small size of the TSS dataset used in this study (Table 2). A selection of k = 7 was
 291 assigned to split the datasets into k groups with an equal number of data points.

292 Table 2: Assessment of fitting error for the proposed TSS model, using k-fold cross validation.

Parameter	k-fold (n)	R2	RMSE	MAE
TSS	7	0.85	0.2159	0.1747

293

294 While these results point to low error levels achieved by the proposed regional TSS retrieval model
 295 (Table-23, Fig-4), caution should be used when applying it to various water types. Water type
 296 classification has been thoroughly described by Balasubramanian et al. (2020) where waters are
 297 classed into Type I (Blue-Green waters), Type II (Green waters), and Type III (Brown waters).
 298 Essentially, the Green-to-Red band ratio is optimised with these datasets corresponding to sediment-
 299 dominated and yellow-substance loaded water conditions. As highlighted by Morel & Belanger (2006),
 300 waters of this type do not have the same spectral characteristics as phytoplankton-rich waters (also
 301 known as Case 1 waters). In addition to the impact on water clarity, sediment particles (often red-
 302 brownish coloured) also tend to enhance the backscattering and absorption properties, especially at
 303 shorter wavelengths (Babin et al., 2003), while the additional presence of coloured dissolved matter

304 (yellow substance) leads to strong absorption properties at short wavelengths. As the TSS retrieval
305 model was developed from samples taken in waters that are bio-optically rich in suspended solids and
306 dissolved organic matter, an application of this TSS model needs to be done cautiously when applying
307 to other water types, particularly those with large concentration of phytoplankton.

308 2.4 Application of TSS retrieval model

309 Daily MODIS-Aqua satellite data from year 2003 to 2019 (total of 6192 individual time slices) were
310 studied with a 2°x 2° spatial resolution (longitude: 109.38, 112.0; latitude: 1.22, 3.35) which covers
311 the southwestern coastal region of Sarawak and southern part of the South China Sea.

312 Atmospherically corrected MODIS-Aqua level 2 reflectance ~~dataproducs~~ (Bailey et al., 2010; NASA
313 Official, n.d.) were retrieved for the application of the TSS model proposed in this study. Negative
314 remote sensing reflectance values, possibly due to failure of atmospheric correction, were filtered out
315 before applying the retrieval model, as expressed in Eq. (2), to map the spatial and temporal
316 distribution of TSS estimates. In addition, averaging of spatial and temporal TSS variation maps in this
317 study was carried out by filtering TSS values with fewer than 10 valid data points over the whole time
318 series, along with application of sigma clipping operation (refer to:
319 https://docs.astropy.org/en/stable/api/astropy.stats.sigma_clip.html).

320 2.4.1 Open Data Cube

321 In this study, the analysis of remote sensing data over large spatial extents and at high temporal
322 resolution was carried out using robust Python libraries and packages run on an Open Data Cube (ODC)
323 platform. Open Data Cube is an open-source advancement in computing technologies and data
324 architectures which addresses the growing volume of freely available Earth Observation (EO) satellite
325 products (Giuliani et al., 2020; Killough, 2019). ODC provides a collection of software which index,
326 manage, and process large EO datasets such as satellite products from the MODIS, Landsat and
327 Sentinel missions (Gomes et al., 2021). These satellite datasets are structured in a multi-dimensional
328 array format, and provide layers of information across latitude and longitude (Open Data Cube, 2021).

329 Leveraging the growing availability of Analysis Ready Data (ARD), and with support from the
330 Committee of Earth Observation Satellites (CEOS) (Killough, 2019), the ODC concept has been
331 deployed in many countries across the world. These existing deployments include Digital Earth Africa
332 (<https://www.digitalearthafrika.org/>), Digital Earth Australia (DEA) (<https://www.dea.ga.gov.au/>),
333 Vietnam Open Data Cube (<http://datacube.vn/>), and Brazil Data Cube ([https://github.com/brazil-data-](https://github.com/brazil-data-cube)
334 [cube](https://github.com/brazil-data-cube)), which provide various time-series datasets of the changing landscape and water content in
335 these specific regions (Giuliani et al., 2020; Gomes et al., 2021; Killough, 2019; Lewis et al., 2017). The
336 ecosystem and architecture of ODC is well explained at opendatacube.org. The codes and tools used
337 in this application drew upon the information provided in various DEA notebooks (Krause et al. (2021),
338 which can be found at <https://github.com/GeoscienceAustralia/dea-notebooks/>.

339 2.5 Precipitation data and computation of river discharge

340 Monthly precipitation values (mm) over the Lupar and Rajang basins were extracted from the Global
341 Precipitation Measurement (GPM) Level 3 IMERG satellite datasets
342 (<https://gpm.nasa.gov/data/imerg>) in order to assess the influence of precipitation in each river basin
343 in relation to TSS concentration at the corresponding river mouth (Supplementary Materials, Fig. S4 –
344 7).

345 Derivation of river discharge (m^3/s) was computed using total precipitation estimates (mm) over each
346 river basin, and multiplied by a surface discharge runoff factor for the studied region (Sim et al., 2020).
347 The surface runoff was estimated to be 60 % of total precipitation (Staub et al., 2000; Whitmore,
348 1984). In this study, the Rajang river basin, as well as the combined basins of the Lupar, Sadong, and
349 Saribas rivers (hereafter referred to as the Lupar basin), were studied for their river discharge rates in
350 relation to TSS release.

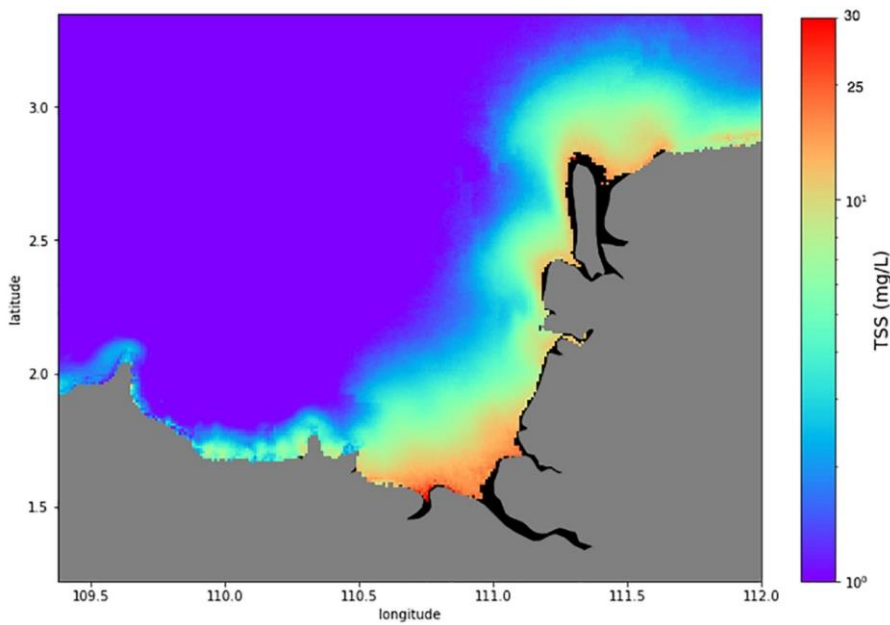
351 3.0 Results & Discussion

352 3.1 Spatial variation of TSS distribution

353 Changes in TSS distribution occur across space and time. The regional TSS remote sensing model
354 calibrated in this study was applied to the time series of MODIS-Aqua data to study the variability of
355 spatial TSS distribution and identify potential hotspot areas susceptible to TSS water quality
356 degradation. The map of average TSS for the Sarawak region was generated (Eq. 2) by averaging all
357 the daily MODIS-Aqua TSS images (2003 to 2019) and is presented in Fig. 45. The results show that
358 the waters in the northeast region of the study area, stretching from the Sadong river to the
359 Rajang/Igan river have seen sustained levels of TSS over the 17 years considered in this study.

360 The temporally averaged spatial distribution map (Fig. 45) shows TSS concentrations in the range of
361 15 – 20 mg/L near the river mouth areas, with widespread TSS plumes extending into the South China
362 Sea (Fig. 5). Based on the Malaysia Marine Water Quality Criteria and Standard (Supplementary
363 Materials, Table S2) (Department of Environment, 2019), these coastal waters fall under Class 1 in
364 relation to their TSS (mg/L) status. This classification indicates that these coastal waters support and
365 preserve marine life in this local region. Yet, several studies have expressed concerns regarding high
366 TSS loadings in riverine waters owing to the impacts of various land use and land cover changes (LULC)
367 (Ling et al., 2016; Tawan et al., 2020). Among these, the Rajang river has been highlighted to be heavily
368 impacted by various LULC activities such as large-scale deforestation and construction of hydropower
369 dams (Alamgir et al., 2020). In situ water quality studies by Ling et al. (2016) reported on high TSS
370 estimates at one of the upstream tributaries of Rajang river, the Baleh river, with TSS readings up to
371 approximately 100 mg/L. Another study by Tawan et al. (2020) reported a significant TSS release
372 reaching to 940,000 mg per day during wet seasons, with maximum TSS concentrations of 1700 mg/L
373 in the upstream tributaries of the Rajang river, particularly at the Baleh and Pelagus rivers. The
374 majority of the upstream tributary rivers were categorised as Class II (during dry season) and Class III
375 (during wet season) waters according to the National Water Quality Index (Supplementary Materials,
376 Table S3) (Department of Environment, 2014), due to increased soil erosion from surrounding LULC
377 activities (Tawan et al., 2020). These local in situ findings provide valuable insights on point source TSS
378 estimates in these LULC change regions. Coupled with our spatial map of average TSS captured by

379 remote sensing technologies, our findings seem to suggest that a large portion of TSS loadings from
380 inland and upstream rivers would have settled and deposited in these river channels and were not
381 completely discharged outwards into the coastal areas, which would have caused major water quality
382 degradation in the corresponding coastal systems.



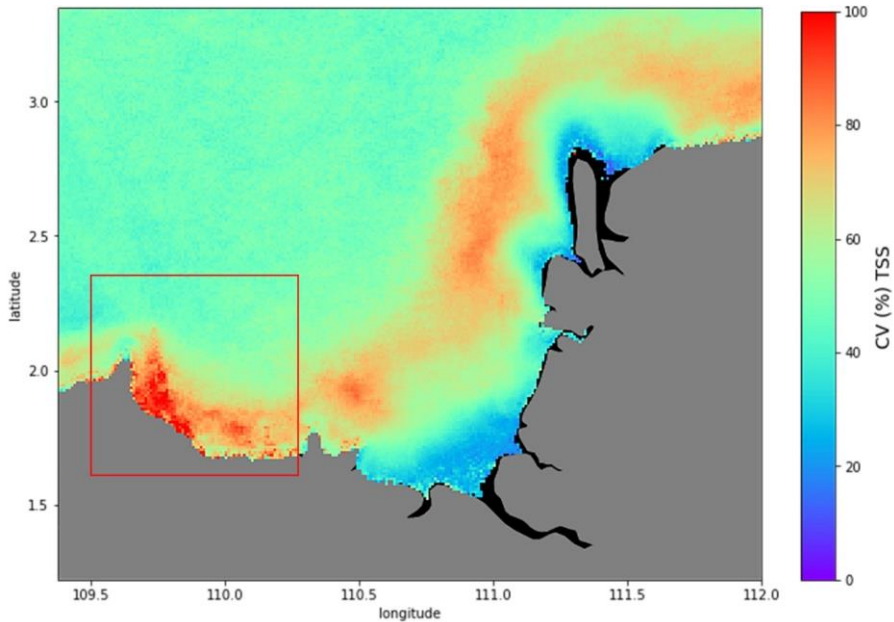
383
384 Fig. 45: Temporally averaged 2°x 2° map of TSS distribution (on a log scale) across the time dimension for each pixel.

385 Historical patterns of TSS concentration were assessed by comparing annual maps of average TSS
386 distribution (Supplementary Materials; Fig. S1), as well as time series of TSS estimates at the Lupar
387 and Rajang river mouths (Supplementary materials; Fig. S2). From our findings, the annual TSS maps
388 further support the observation where TSS release was evident at Lupar and Rajang/Igan river mouths
389 from 2003 till 2019, which points to Class I of local water quality standards in relation to TSS (mg/L)
390 status. This was found to consistently occur every year. Furthermore, the TSS trend study showed that
391 both the Lupar and Rajang river mouth points have a gradual increase of TSS concentration over the

392 17 years (Supplementary materials; Fig. S2). This increasing trend was, however, not statistically
393 significant ($p = 0.43$ for Lupar, and $p = 0.15$ for Rajang).

394 Moreover, a map of the TSS coefficient of variation (CV) was computed to identify areas with a high
395 degree of relative TSS variation over time (Fig. 56). Here again, the map of CV (%) was produced by
396 aggregation of the daily MODIS-Aqua images (6192 time steps) from 2003 until 2019. Figure 56 shows
397 that the Samunsam-Sematan coastal region (as highlighted by the red box) exhibits an increased level
398 of TSS distribution variability, with a recorded CV of more than 90 %.

399 The Samunsam-Sematan coastal region contains near-pristine mangrove forests which are sheltered
400 from major LULC activities, as compared to other studied sites. Samunsam-Sematan is also well-known
401 locally as a recreational hotspot with coral reefs and various national parks (Sarawak Tourism Board,
402 2021). Data from the Centre for International Forestry Research (CIFOR) Forrest Carbon database
403 (CIFOR, n.d.) revealed that there was more than double the amount of total forest loss (approx. 5,000
404 Ha) recorded in Lundu, a nearby township in the Sematan area in 2011 as compared to the previous
405 years. Deforestation activities, regardless of their scale, can inevitably promote sediment loss and soil
406 leaching into the nearby river systems (Yang et al., 2002). Important information regarding the
407 variability in water quality (as shown in Fig. 56) can provide support to local authorities and relevant
408 agencies in order to identify vulnerable areas that need to be monitored closely, such as the Lundu-
409 Sematan region in this case. The CV map thus offers interesting insights into how TSS distribution can
410 vary across large spatial areas, which can ultimately impact local socio-economic activities in this
411 region (Lee et al., 2020b).



412

413 Fig. 56: Map of CV (%) calculated from the daily time series of MODIS-Aqua satellite images from 2003 until 2019.

414 3.2 Temporal variation of TSS distribution

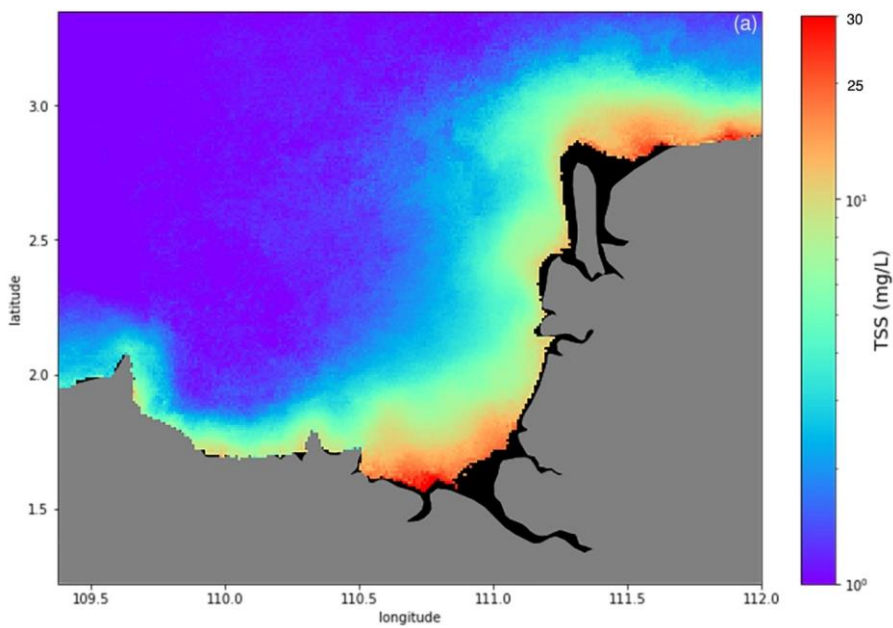
415 On a temporal scale, the northeast (NE) monsoon period shows a distinct difference in the widespread
 416 intensity of TSS distribution as compared to the southwest (SW) monsoon period, along the Sarawak
 417 coastline over the 17 years of the considered time series (Fig. 67). Mapping of temporal variations
 418 between monsoons using time-series MODIS-Aqua datasets can provide an improved understanding
 419 on the intensity of monsoonal patterns in driving the TSS distribution in this region. As shown in Figure
 420 67, TSS release can be seen to extend further into the open ocean South China Sea region during the
 421 NE monsoon periods (Fig. 67a) in comparison to the SW monsoon periods (Fig. 67b).

422 In addition, the differences in TSS release between the NE and SW monsoons $((NE-SW)/NE \times 100)$ were
 423 mapped as shown in Fig. 67c. Widespread TSS plumes are detected at Lundu/Sematan region ($>80\%$
 424 relative difference in TSS concentration) on the southwest side of the study area, while substantial
 425 TSS plumes are observed in front of the Igan river channel, with more than 50% relative difference in

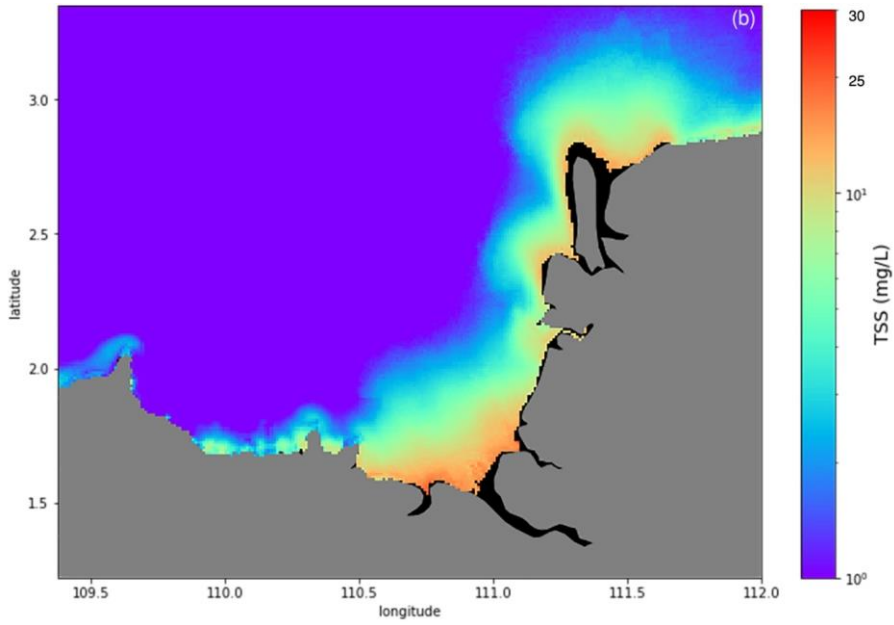
426 TSS concentration in comparison to SW monsoon periods. Sadong coastal area is observed to receive
427 considerable TSS loadings (> 30%) during NE monsoon periods.

428 These coastal areas would thus be more likely to be impacted by the TSS release during the NE
429 monsoon periods. These findings further strengthen the evidence that tropical rivers are majorly
430 impacted by climatic variability such as monsoonal patterns, as highlighted in a study at Baleh river in
431 Sarawak (Chong et al., 2021). This suggests that monsoon rains, which typically last for several months,
432 play an integral role in driving the discharge of TSS in tropical rivers.

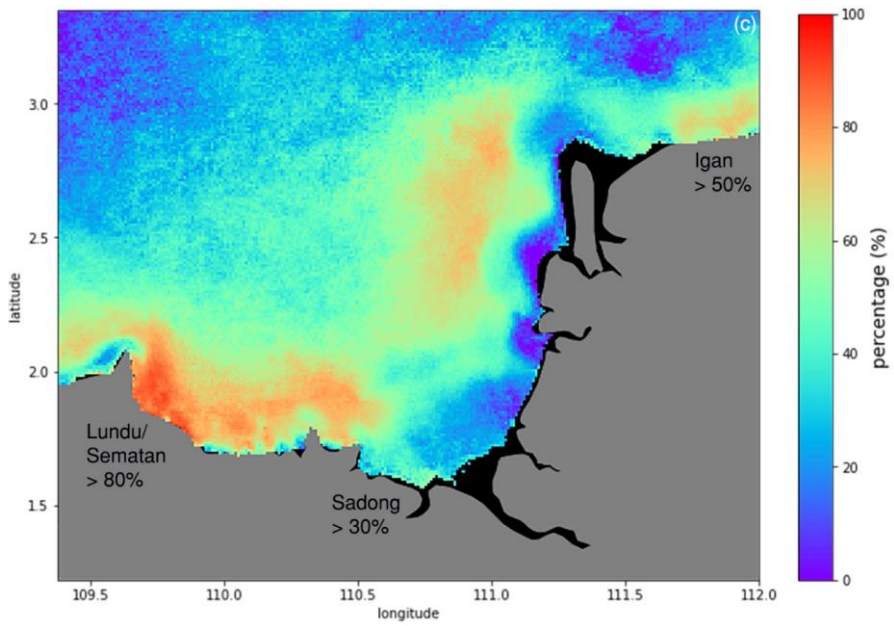
433



434



435



436

437 Fig. 62: Long-term average of TSS estimates (mg/L) during the Northeast monsoon (a), and the Southwest monsoon (b). The

438 map of TSS difference between the Northeast and Southwest monsoon periods, computed in relative percentage (%), is
439 shown in (c).

440 Several climatic studies in the Borneo region highlighted 2009 as a year with extreme rainfall events
441 which caused major floods in Sarawak (Dindang et al., 2011; Sa'adi et al., 2017), while drought events
442 were reported in 2014 (Bong and Richard, 2020). Hence, in this study, TSS dynamics for the Lupar and
443 Rajang rivers were studied by assessing the variation of TSS values at selected pixels in relation to
444 monsoonal rainfall patterns in 2009 and 2014 (Supplementary Materials; Fig. S3).

445 Generally, the results show fluctuations of TSS concentrations across the NE and SW monsoon periods
446 in relation to precipitation values (Fig. 7&a – d). Based on Fig. 7&a, monthly precipitation values
447 recorded for the Lupar river basin in 2009 showed a clear decreasing trend from the NE monsoon
448 period (wet season) to the SW monsoon period (dry season), while gradually increasing approaching
449 the year end's NE monsoonal period. A similar precipitation pattern was observed for the Rajang river
450 basin during the same year (Fig. 7&c).

451 However, these results also show that the TSS distribution (mg/L) at the Lupar river mouth seems to
452 show no distinct trend of decreasing TSS concentration estimates during the SW monsoon period in
453 year 2009 (Fig. 7&a) in relation to its precipitation values. Additionally, a sharp rise of TSS release can
454 be seen in the month of May (beginning of SW monsoon period), with a near equivalent intensity of
455 TSS release during the NE monsoon period. This observation may potentially be caused by the lag
456 between the time of rainfall events occurring during NE monsoon periods and TSS release entering
457 the coastal river regions. A similar observation was described by Sun et al. (2017a) suggesting that
458 riverine outputs could take several days, and even up to one month to reach the coastal river points.
459 Considering the occurrence of extreme rainfall events in 2009, our findings are in agreement with
460 these processes as TSS concentrations generally exhibit a similar intensity throughout the NE and SW
461 monsoonal periods for the Lupar river (Fig. 7&a). This result could suggest that the occurrence of

462 extreme rainfall events, as reported for the year 2009, can exert a much larger impact on TSS
463 transportation and release in monsoon-driven tropical rivers.

464 Drought events in 2014 can be seen to impact the precipitation values at both the Lupar (Fig. 7&b) and
465 Rajang river basins (Fig. 7&d). There ~~are~~ no apparent patterns of decreasing precipitation values
466 during the shift of NE to SW monsoonal periods as compared to the year 2009, for either river basin.
467 However, precipitation values were found to increase sharply during the year end NE monsoon period
468 for both river basins. The TSS concentrations at the Lupar coastal river points were found to be the
469 highest during the NE monsoon period earlier in January and February of 2014 (Fig. 7&b). This may be
470 due to the temporal lag in the transition of TSS discharge into the coastal systems arising from the
471 prior months (November and December) in the previous year, when higher rainfall events were
472 typically observed in this region (Gomyo and Koichiro, 2009; Tangang et al., 2012). The TSS distribution
473 at both Lupar and Rajang coastal river points showed no distinct trend in relation to the precipitation
474 values throughout a period of ten months until November 2014. These findings suggest that coastal
475 areas in the Borneo region may not be experiencing critical water quality degradation during dry
476 seasons.

477

478

479

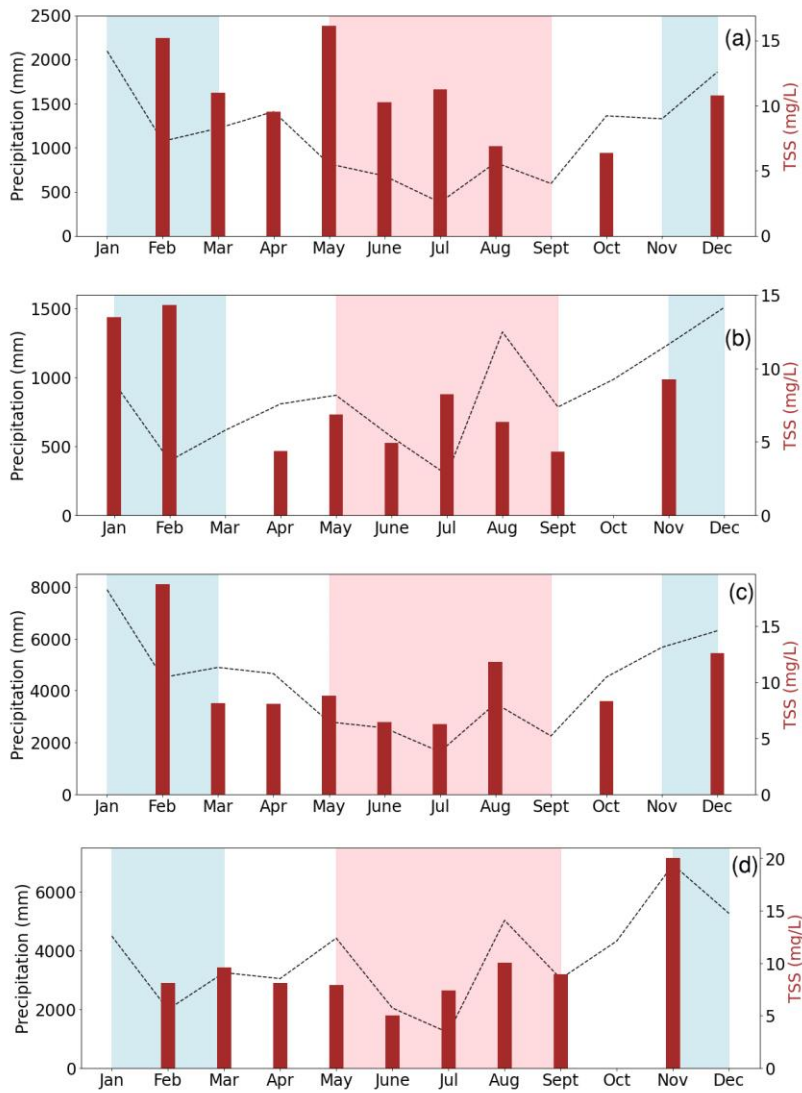
480

481

482

483

484



485
 486 Fig. 7.9: Temporal analysis of precipitation (mm) from the Lupar and Rajang river basins in relation to TSS concentrations
 487 (mg/L) during the NE and SW monsoon periods at the Lupar ((a): 2009; (c): 2014) and Rajang ((b): 2009; (d): 2014) coastal
 488 river point. The NE monsoon months are highlighted with a blue background; those of the SW monsoon with a pink
 489 background, and intermonsoon periods with a white background.

490 3.2.1 Temporal TSS anomalies

491 Considering the temporal variation recorded across monsoons, maps of relative TSS anomalies were
492 calculated for each year as the difference with respect to the long-term TSS mean (Fig. 45), in order
493 to detect changes of TSS distribution occurring annually (Fig. 89). As shown in Figure 89, year 2010
494 experienced a distinct increase of TSS distribution (approximately 100 %), with widespread pattern
495 extending into open ocean waters, in comparison to the long-term TSS mean. This finding provides an
496 interesting insight into the effects of extreme rainfall events as recorded in year 2009, which could
497 potentially intensify TSS release into the coastal and open ocean waters. The effects of TSS release
498 can still be seen a year after the extreme rainfall events in this region. This observation could provide
499 further evidence that the impacts of the TSS release from the land into rivers and coastal systems may
500 only take effect after a substantial period, as previously observed by Sun et al. (2017a).

501 Figure 89 further reveals an interesting pattern of TSS increase in the Samunsam-Sematan region from
502 year 2004 until 2019, with exceptions during the years 2007 and 2008. As previously highlighted in
503 Section 3.1, the Samunsam-Sematan region has been observed to be a vulnerable coastal area with
504 respect to TSS water quality degradation. From the annual map of TSS anomalies (Fig. 89), we can see
505 that the TSS distribution has the tendency to accumulate in the Samunsam-Sematan region, as
506 opposed to being distributed into the open ocean waters. This may be due to the geographical and
507 hydrological characteristics of these coastal regions (Martin et al., 2018), as the TSS release may be
508 sheltered from open ocean waters, and hence induce a higher TSS accumulation in these coastal
509 regions.

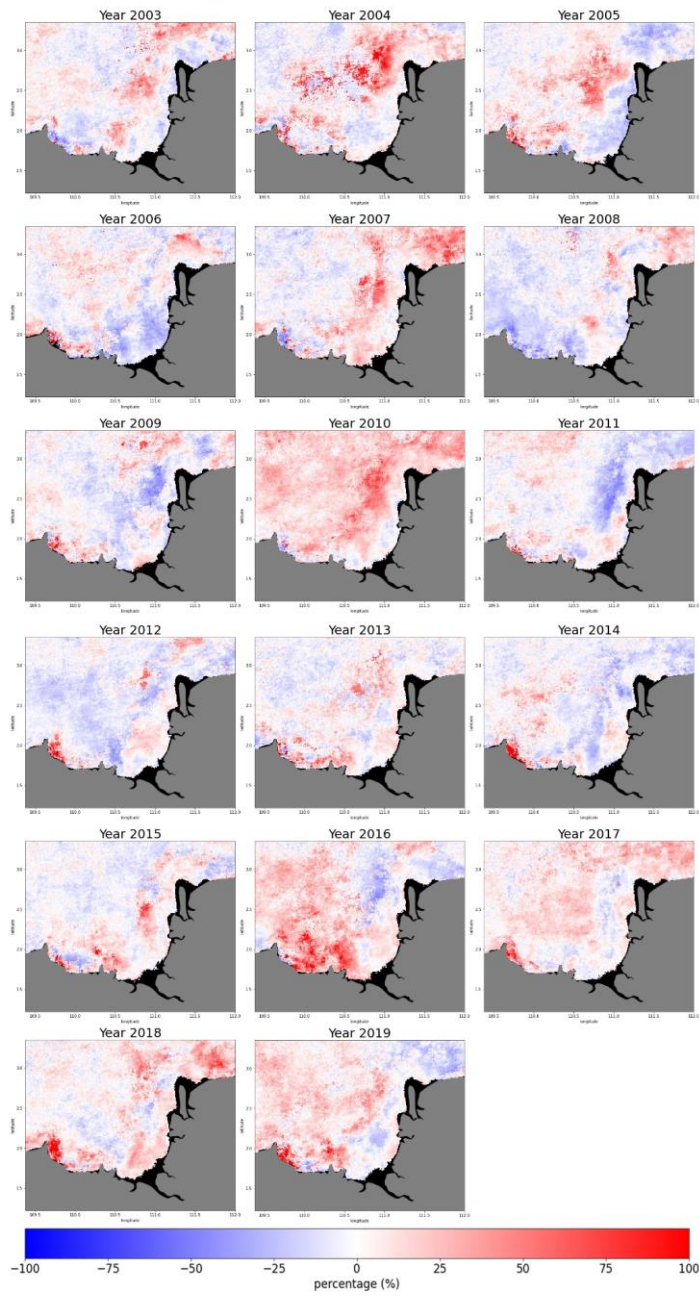
510

511

512

513

514



515

516 Fig. 89: Map of relative TSS distribution anomalies with respect to the long-term mean, represented as percentage (%),
 517 from year 2003 until 2019.

518 3.3 Hydrological factors driving TSS discharge

519 Apart from the influence of monsoonal patterns, hydrological factors such as the river discharge are
520 among the dominant drivers in transporting various water constituents in riverine and coastal systems
521 (Loisel et al., 2014; Petus et al., 2014; Sun, 2017b; Verschelling et al., 2017). In this study, river
522 discharge from the Lupar and Rajang basins was estimated and investigated.

523 Yearly river discharge estimates from 2003 until 2019 were investigated to assess its effect on the TSS
524 distribution (Fig. 940) represented by changes in TSS values for pixels located at each Lupar and Rajang
525 coastal river points (Supplementary Materials, Fig. S3). Figure 940a shows that river discharge values
526 in the Lupar basin (750 to 1050 m³/s) are approximately twice lower than the Rajang river discharge
527 (Fig. 940b), which recorded a range of 3,200 to 4,000 m³/s.

528



529

530 Fig. 940: Time-series analysis of river discharge (m³/s) in relation to TSS concentrations (mg/L) for the Lupar (a) and Rajang
531 (b) basins from year 2003 to 2019. Note the differing scaling on the ordinate axes in each plot.

532

533 Discrepancies between TSS estimates and river discharge were identified in both the Lupar and Rajang
534 coastal regions in these annual time-series, where river discharge was inversely correlated with TSS
535 estimates. These discrepancies are not uncommon, as previously highlighted in a study by Zhan et al.
536 (2019). Especially in 2010 for the Lupar river, Fig. 9a shows a drop in TSS release in relation to the
537 steady increase of river discharge from the river basin. In 2011 and 2012, a negative correlation can
538 be seen between river discharge and TSS estimates, while in subsequent years from 2013 until 2015,
539 there is a clear positive correlation. The TSS output from the Lupar basin recorded a correlation
540 coefficient of $r = 0.15$, while river discharge from the Rajang basin did not substantially influence the
541 TSS release either, with $r = 0.27$ throughout the seasons (Supplementary Materials, Fig. S8a and b).
542 Although there is no obvious environmental factor that would explain these discrepancies and poor
543 correlation between river discharge and TSS estimates in this study, these findings may imply a
544 complex interaction and process between human interventions, such as damming and deforestation
545 activities, which are largely occurring within the Rajang river basin (Alamgir et al., 2020), as well as
546 varying hydrological and atmospheric conditions (wind and tidal mixing) in regulating TSS dynamics in
547 a localised region (Espinoza Villar et al., 2013; Fabricius et al., 2016; Ramaswamy et al., 2004; Valerio
548 et al., 2018; Wu et al., 2012; Zhan et al., 2019; Zhou et al., 2020).

549 ~~Discrepancies between TSS estimates and river discharge were identified in both the Lupar and Rajang~~
550 ~~coastal regions in these annual time-series, where river discharge was inversely correlated with TSS~~
551 ~~estimates. These discrepancies are not uncommon, as previously highlighted in a study by Zhan et al.~~
552 ~~(2019). Especially in 2010 for the Lupar river, Fig. 10a shows a drop in TSS release in relation to the~~
553 ~~steady increase of river discharge from the river basin. In 2011 and 2012, a negative correlation can~~
554 ~~be seen between river discharge and TSS estimates, while in subsequent years from 2013 until 2015,~~
555 ~~there is a clear positive correlation. Although there is no obvious environmental factor that would~~
556 ~~explain these discrepancies, these findings may imply a complex interaction between human~~
557 ~~interventions, such as damming and deforestation activities, as well as varying hydrological and~~

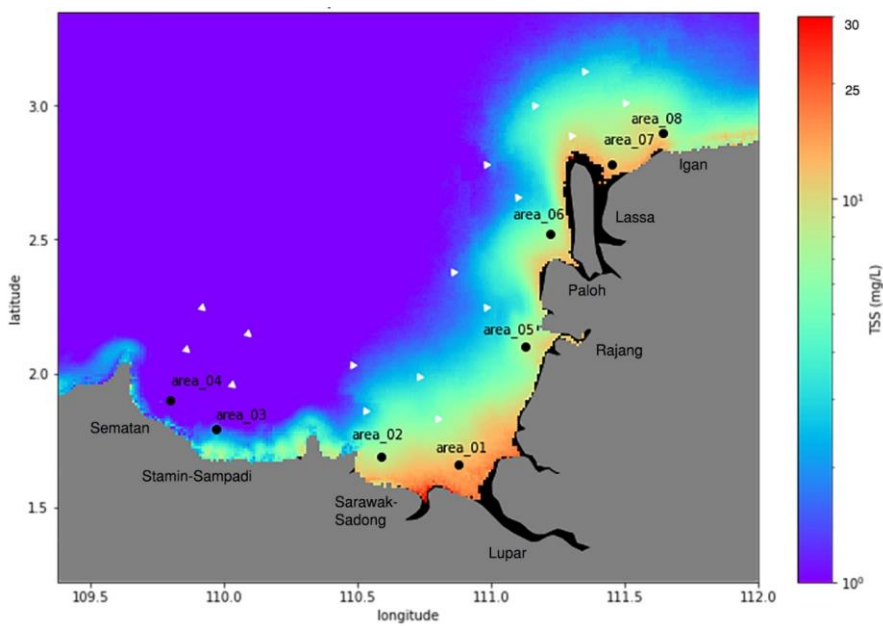
558 atmospheric conditions (wind and tidal mixing) in regulating TSS dynamics (Wu et al., 2012; Zhan et
559 al., 2019).

560 The correlation between TSS release and river discharge at both the Lupar and Rajang coastal areas
561 was further evaluated in this study. Even though river discharge has been shown (in other global
562 studies) to be one of the dominant factors in moderating TSS release (Fabricius et al., 2016; Tilburg et
563 al., 2015; Verschelling et al., 2017; Wu et al., 2012), the TSS distribution at both the Lupar and Rajang
564 river mouths in this study can be seen to be only poorly correlated with river discharge from each river
565 basin (Supplementary Materials, Fig. S8a and b). The TSS output from the Lupar basin recorded a
566 correlation coefficient of $r = 0.15$, while river discharge from the Rajang basin did not substantially
567 influence the TSS release either, with $r = 0.27$ throughout the seasons. Coupled with tidal mixing
568 processes (Ramaswamy et al., 2004; Zhou et al., 2020), it is possible that human activities such as
569 deforestation, logging, and construction of dams, which are largely occurring within the Rajang basin
570 (Alamgir et al., 2020), are mainly driving TSS release and resuspension in this area. This indicates that
571 although TSS release is regarded to be highly dependent on, and controlled by river discharge patterns,
572 this interaction often represents an intricate process linked to local hydrodynamics process and socio-
573 economic conditions (Espinoza Villar et al., 2013; Fabricius et al., 2016; Valerio et al., 2019; Zhan et al.,
574 2019).

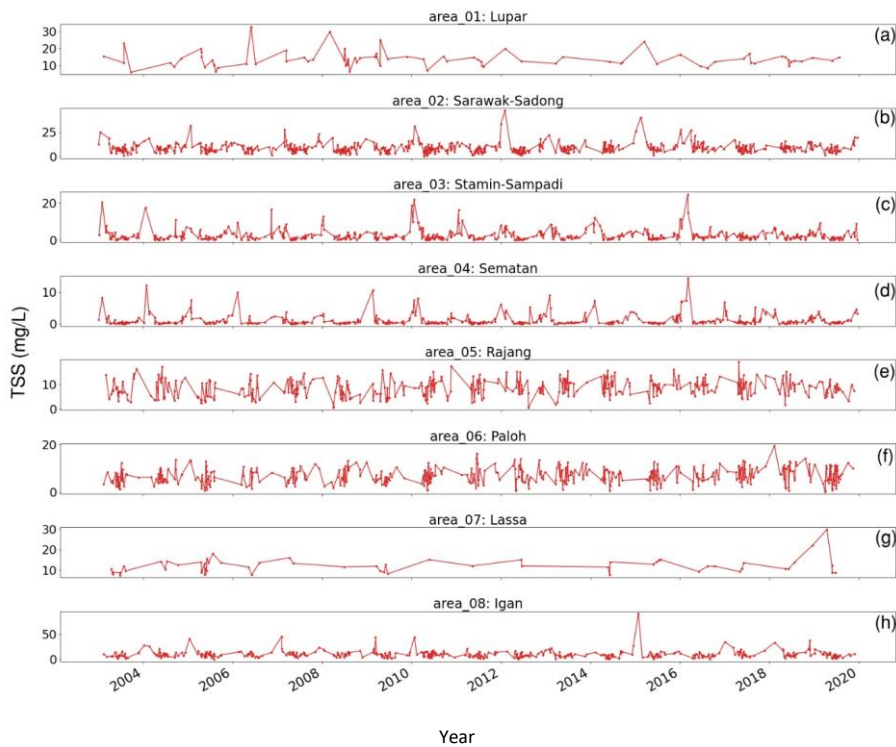
575 3.4 Variability of TSS across coastal waters

576 As previously observed in Fig. 45, varying river plumes of TSS were evidently detected within the
577 coastal regions of the study area. Notably, coastal river plumes represent important factors driving
578 the transport of water constituents and nutrients from coastlines to the open oceanic systems (Petus
579 et al., 2014). To assess this and evaluate the water quality status in coastal zones, the spatial extent
580 of TSS release was investigated along transects covering the territorial (12 nautical miles) and open
581 water areas (24 nautical miles) of the Sarawak region (Fig. 104).

582 A total of eight coastal points were selected based on the main river mouths located in the southwest
583 region of Sarawak. Transect points are positioned in a line starting at the coastal river points to
584 examine the variations of TSS distribution across different water zones. Daily changes in TSS
585 concentration for each pixel located in front of the river mouths were plotted from 2003 until 2019
586 (Fig. 112).



587
588 Fig. 104: Map of average TSS estimates (mg/L) with indicators at eight main river mouths and their transect, extending from
589 coastal waters into territorial and open ocean systems. Indicators of each river mouths are as follows: area_01 – Lupar river;
590 area_02 – Sarawak-Sadong river; area_03 - Stamin-Sampadi river i; area_04 – Sematan river; area_05: Rajang river; area_06:
591 Paloh river; area_07: Lassa river; and area_08: Igan river).



592
 593 Fig. 112: Graphs of daily TSS estimates (mg/L) recorded at eight river mouth points from 2003 to 2019. Presentation of each
 594 river mouths is as follows: a) area_01; b) area_02; c) area_03; d) area_04; e) area_05; f) area_06; g) area_07; h) area_08.
 595 Note the different TSS scales in each plot.

596 From the high temporal resolution graphs in Fig. 112, no general trend of TSS concentration can be
 597 identified over the years at each coastal point. It is worth highlighting that the daily temporal
 598 resolution was particularly affected at coastal points located in front of the Lupar (area_01) and Lassa
 599 (area_07) river mouths due to various pixel data quality issues in these areas. Nonetheless, more than
 600 80 satellite images with minimum cloud coverage at these two locations were processed, while the
 601 remaining coastal points had a total of more than 400 satellite images to assess the temporal trend.
 602 Despite the fact that no distinct upward or downward trend was observed, our findings indicate that
 603 several river mouths are actively discharging and accumulating substantial TSS amounts over the

604 period of years, while resuspension of bottom sediments induced by wind and tidal cycle is another
605 factor contributing to the variation of TSS values (Park, 2007; Song et al., 2020).

606 The coastal region of the Sarawak-Sadong river (area_02) shows relatively high TSS distribution
607 patterns with some periods recording an estimate of over 30 mg/L of TSS concentration. This is in
608 agreement with the localised characteristics of the Sarawak river basin which essentially drains
609 through the populated Kuching area with high industrial and development activities in the capital city
610 of Sarawak (DID, 2021b). In comparison with other river mouth points, a steady TSS concentration
611 below 20 mg/L was recorded across the Stamin-Sampadi (area_03), Sematan (area_04), Rajang
612 (area_05), and Paloh (area_06) river mouths. Consistently high TSS values in the daily plots were
613 recorded at the Lupar (area_01) and Pulau Bruit-Lassa (area_07) river mouths, with estimates of up to
614 30 mg/L on a near-daily basis. Similar high TSS amounts from the Igan (area_08) river mouth, situated
615 northeast side of the Pulau Bruit-Lassa region, were observed in Cherukuru et al. (2021) and Staub et
616 al. (2000).

617 Although the daily TSS estimates at each river point are in line with various reported studies (Chen et
618 al., 2011, 2015b; Kim et al., 2017; Mungen et al., 2020; Zhang et al., 2010a), these estimates can be
619 expected to be much higher for sampling points much closer to the river mouths. The selection of
620 coastal river points in this study was made to minimize the gaps with respect to various pixel data
621 quality issues in the MODIS-Aqua datasets, and hence, the use of coastal river points closer to shore
622 would have been impractical.

623 These findings further suggest that higher TSS loadings within the coastal river areas would have been
624 diluted or deposited while travelling to the open oceanic systems as they are weakly impacted by river
625 discharge in relation to offshore distance (Espinoza Villar et al., 2013). This understanding can be
626 observed in Fig. 123, which shows a progressively decreasing TSS estimates at each transect in relation
627 to the distance from the shore. Generally, TSS estimates in coastal zones (first transect point) show
628 considerably higher TSS concentrations. When moving outwards to territorial waters (second transect

629 point), TSS concentration estimates decrease by nearly 50 % before travelling to open ocean systems
630 (third transect point), except for the northeast regions (area_07 and area_08) which seem to show
631 large extension of TSS plumes to the open ocean waters, as also highlighted by Cherukuru et al. (2021).
632 A reversed trend can be seen in the plot corresponding to the Sematan coastal river systems, although
633 the absolute increase in TSS estimates across water zones (0.2 mg/L in total) here is only marginal (Fig.
634 13d). Such slight trend in TSS retrievals recorded (Figure 12) generally offers a synoptic understanding
635 of the trend conditions, considering such small variabilities in TSS retrieval were captured by the
636 power function TSS retrieval model given its extent of uncertainties (Table 2).

637

638

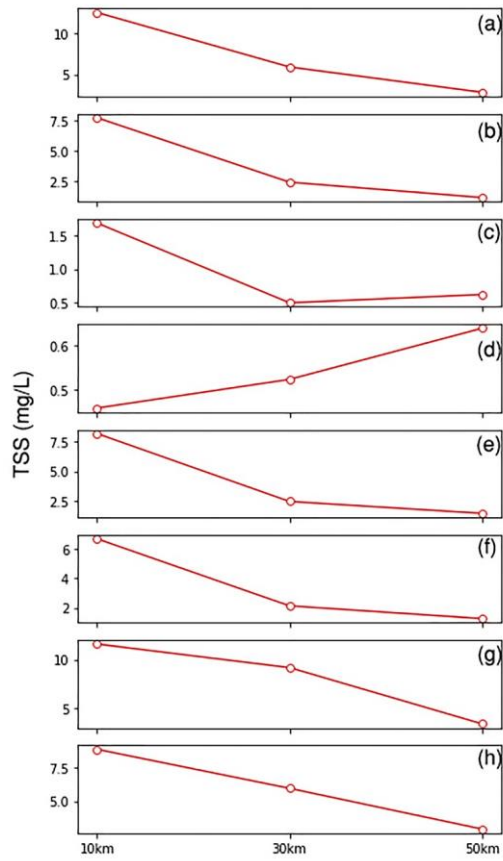
639

640

641

642

643



644

645 Fig. 123: Average TSS estimates (mg/L) computed from 2003 to 2019 for each of the eight rivers (area_01: (a), area_02: (b);
 646 area_03: (c); area_04: (d); area_05: (e); area_06: (f); area_07: (g); and area_08: (h)) and their relevant transect points with
 647 distance of 10 km (coastal waters), 30 km (territorial waters) and 50 km (open ocean waters) from the shoreline. Note the
 648 varying TSS scales on the ordinate axes in each plot.

649

650

651

652

653 3.5 Discussion of TSS implications for coastal waters

654 High discharge of TSS into coastal environments can lead to adverse environmental and ecological
655 implications. The presence of TSS affects water transparency and light availability within the surface
656 waters (Dogliotti et al., 2015; Nazirova et al., 2021; Wang et al., 2021). Among others, TSS affects the
657 photosynthesis activities of algae and macrophytes. TSS in water creates a reduction in light
658 penetration, which impacts the primary production of aquatic organisms and hence the support
659 system of marine life (Bilotta and Brazier, 2008; Loisel et al., 2014).

660 Additionally, TSS exerts an influence on zooplankton communities. Reduction in water clarity induces
661 changes in the zooplankton's biomass volume and composition, while TSS may carry a level of toxicity
662 which affects zooplankton through ingestion (Chapman et al., 2017; Donohue and Garcia Molinos,
663 2009). Apart from that, accumulation and deposition of sediments decreases the level of dissolved
664 oxygen (DO) at the bottom of the water column, and subsequently impacts the benthic invertebrate
665 groups (Chapman et al., 2017). Moreover, substantial TSS deposition tends to cause harmful physical
666 effects to these benthic groups, such as abrasion, and even clogging by sediment particles (Chapman
667 et al., 2017; Langer, 1980).

668 As a result of these TSS effects on lower trophic levels, fish communities are critically impacted, with
669 a reduction in diversity and abundance (Kemp et al., 2011). While fish communities learn to adapt to
670 a range of TSS loads (Macklin et al., 2010), increase of TSS concentrations often depletes DO
671 concentrations in the water system and causes stress towards these aquatic communities (Henley et
672 al., 2000). Fish populations tend to decrease, as feeding and growth rates are negatively impacted
673 (Shaw and Richardson, 2001; Sutherland and Meyer, 2007).

674 Threats to coral reefs have been linked to sediment-induced stress which often leads to a reduction
675 in the coral's growth and metabolic rate, as well as impending mortality (Erftemeijer et al., 2012;
676 Gilmour et al., 2006; Risk and Edinger, 2011). Factors of coral stress are driven by nutrient-rich
677 sediments and microbes which are being carried by TSS, with impacts on the health of coral tissues

678 (Hodgson, 1990; Risk and Edinger, 2011; Weber et al., 2006). A reduction in light availability impedes
679 the development of corals (Anthony and Hoegh-Guldberg, 2003; Rogers, 1979; Telesnicki and
680 Goldberg, 1995). A combined increase in TSS and nutrient loadings contribute to the decrease of coral
681 species diversity and composition (Fabricius, 2005).

682 Essentially, presence of TSS in water systems has impacts across various aquatic biota. With the severe
683 implications of decreased fish population, this could lead to a disruption of fisheries activities by local
684 communities, especially considering that more than 80 % of the Sarawak population is living in the
685 coastal areas (DID, 2021a). Coral reefs are important coastal biodiversity assets to the Sarawak region,
686 especially around the Talang-Talang and Satang islands on the southwest coast of Sarawak (Long,
687 2014). With the use of remote sensing technologies in monitoring Sarawak coastal water quality, the
688 approach presented in this paper provides digital-based solutions to assist relevant authorities and
689 local agencies to better manage the Sarawak coastal waters and their resources.

690 4.0 Conclusion

691 In this study, a regional empirical TSS retrieval model was developed to analyse TSS dynamics along
692 the southwest coast of Sarawak. The empirical relationship between in situ reflectance values, $Rrs(\lambda)$,
693 and in situ TSS concentrations was established using a green-to-red band ratio using the MODIS-Aqua
694 $Rrs(530)$ and $Rrs(666)$ reflectance bands. An evaluation of the TSS retrieval model was carried out with
695 error metric assessment, which yielded results of bias = 1.0, MAE = 1.47 and RMSE = 0.22 in mg/L
696 computed in log₁₀-transformed space prior to calculation. A statistical analysis using a k-fold cross
697 validation technique (k = 7) reported low error metrics (RMSE = 0.2159, MAE = 0.1747).

698 The spatial TSS distribution map shows widespread TSS plumes detected particularly in the Lupar and
699 Rajang coastal areas, with average TSS range of 15 – 20 mg/L estimated at these coastal areas. Based
700 on the spatial map of the TSS coefficient of variation, large TSS variability was identified in the
701 Samunsam-Sematan coastal areas (CV > 90 %). The map of temporal variation of TSS distribution
702 points to a strong monsoonal influence in driving TSS release, with large differences identified

703 between the northeast and southwest monsoon periods in this region. From the annual TSS anomalies
704 maps, the Samunsam-Sematan coastal areas demonstrated strong TSS variation spatially, while
705 widespread TSS distribution with nearly 100 % of TSS increase in comparison to long term mean was
706 observed in 2010. Furthermore, our study on river discharge in relation to TSS release demonstrated
707 a weak relationship at both the Lupar and Rajang coastal river points. Study on the TSS variability
708 across coastal river mouths implied that higher TSS loadings in the coastal areas are potentially being
709 deposited or diluted in the process of being transported into the open ocean waters, with varying
710 magnitude at several coastal river points.

711 Overall, these coastal areas of Sarawak are dominantly categorised as Class I quality, which remain
712 within local quality standards to support various marine and socio-economic activities in this region.
713 Our findings in the southwest coastal areas (Sematan and Stamin-Sampadi) showed that the coral
714 reefs there can be well-maintained with negligible impacts from TSS loadings. However, it is important
715 to highlight the various human activities that are widely ongoing in this region, which include
716 deforestation and logging activities (Alamgir et al., 2020; Hon and Shibata, 2013; Vijith et al., 2018).
717 Impacts from these activities in Sarawak can potentially aggravate current soil erosion issues, and
718 ultimately induce more soil leaching and runoff from land to water systems, especially during heavy
719 rainfall events (Ling et al., 2016; Vijith et al., 2018). As a result, human activities may have a greater
720 influence on driving riverine sediments than climatological factors, as reported by Song et al. (2016).
721 As such, this work presents the first observation of TSS distributions at large spatial and temporal
722 scales in Sarawak's coastal systems, and of the potential associated impacts on the South China Sea.

723 While the ~~The~~ findings derived from this work can be used to support local authorities in assessing TSS
724 water quality status in the coastal areas of concern, ~~the developed TSS retrieval model presents~~
725 ~~several limitations, and to enhance coastal management and conservation strategies. Given the~~
726 ~~consideration that the model was developed from sediment and organic matter rich waters, the model~~
727 ~~is not transferable to other optical water types. This model is most applicable to be applied in waters~~

728 with similar optical characteristics such as the southwest coastal waters of Sarawak region. There is a
729 need to further optimize the model with larger datasets covering more coastal water points, as well
730 as data points from varied seasonal patterns, to improve its performance on a spatial and temporal
731 scale. As these data points were collected within the southwest region of Sarawak's coastal waters,
732 further testing and validation of the model in other regions of Sarawak's coastal waters is essential to
733 develop a more robust TSS retrieval model and be applied to a broader regional scale. The application
734 of remote sensing technologies is of great benefit in the development of sustainable sediment
735 management in the Sarawak coastal region, as demonstrated in this study.

736 With the demand to enhance coastal management and conservation strategies in Sarawak's coastal
737 waters, the application of remote sensing technologies, as demonstrated in this study, is a great
738 benefit in the development of sustainable sediment management in the Sarawak coastal region.

739 Data availability. The dataset related to this study is available as supplement to this paper.

740 Author contributions. Conceptualization, J.C., N.C., E.L., and M.M.; Formal analysis, J.C., N.C. and E.L.;
741 Funding acquisition, M.M, N.C., and A.M.; Investigation, J.C., N.C., E.L., M.P., P.M., A.M., and M.M.;
742 Methodology, J.C., N.C., E.L., and M.M.; Resources, J.C., N.C., E.L., M.P., and M.M.; Validation, J.C.,
743 N.C., E.L. and M.M.; Writing— original draft, J.C.; Writing—review & editing, J.C., N.C., E.L., P.M., and
744 M.M.; Supervision, M.M., N.C., and A.M.; Project administration, M.M., A.M., and N.C.

745 Competing interests. The authors declare that they have no conflict of interest.

746 Acknowledgement. We thank Sarawak Forestry Department and Sarawak Biodiversity Centre for
747 permission to conduct collaborative research in Sarawak under permit numbers NPW.907.4.4(Jld.14)-
748 161, SBC-RA-0097-MM, and Park Permit WL83/2017. We would like to extend our gratitude to all the
749 boatmen and crew during all the field expeditions. Special thanks to Pak Mat and Minhad during the
750 western region sampling, and Captain Juble, as well as Lukas Chin, during the eastern region cruises.
751 We are appreciative to members of AQUES MY for their kind participation and involvement, especially

752 to Ashleen Tan, Jack Sim, Florina Richard, Faith Chaya, Edwin Sia, Faddrine Jang, Gonzalo Carrasco,
753 Akhmetzada Kargazhanov, Noor Iskandar Noor Azhar, and Fakharuddin Muhamad. The study was
754 supported by Australian Academy of Sciences under the Regional Collaborations Programme, Sarawak
755 Multimedia Authority (Sarawak Digital Centre of Excellence) and Swinburne University of Technology
756 (Swinburne Research Studentship).

757

758 References:

- 759 Ahn, Y. and Shanmugam, P.: Derivation and analysis of the fluorescence algorithms to estimate
760 phytoplankton pigment concentrations in optically, , doi:10.1088/1464-4258/9/4/008, 2007.
- 761 Alamgir, M., Campbell, M. J., Sloan, S., Engert, J., Word, J. and Laurance, W. F.: Emerging challenges
762 for sustainable development and forest conservation in Sarawak, Borneo, PLoS One, 15(3), 1–20,
763 doi:10.1371/journal.pone.0229614, 2020.
- 764 Alcântara, E., Bernardo, N., Watanabe, F., Rodrigues, T., Rotta, L., Carmo, A., Shimabukuro, M.,
765 Gonçalves, S. and Imai, N.: Estimating the CDOM absorption coefficient in tropical inland waters
766 using OLI/Landsat-8 images, Remote Sens. Lett., 7(7), 661–670,
767 doi:10.1080/2150704X.2016.1177242, 2016.
- 768 Anthony, K. R. N. and Hoegh-Guldberg, O.: Kinetics of photoacclimation in corals, *Oecologia*, 134(1),
769 23–31, doi:10.1007/s00442-002-1095-1, 2003.
- 770 Babin, M., Stramski, D., Ferrari, G. M., Claustre, H., Bricaud, A., Obolensky, G. and Hoepffner, N.:
771 Variations in the light absorption coefficients of phytoplankton, nonalgal particles, and dissolved
772 organic matter in coastal waters around Europe, , 108, doi:10.1029/2001JC000882, 2003.
- 773 Bailey, S. W., Franz, B. A. and Werdell, P. J.: Estimation of near-infrared water-leaving reflectance for
774 satellite ocean color data processing, *Opt. Express*, 18(7), 7521, doi:10.1364/oe.18.007521, 2010.
- 775 Balasubramanian, S. V., Pahlevan, N., Smith, B., Binding, C., Schalles, J., Loisel, H., Gurlin, D., Greb, S.,
776 Alikas, K., Randla, M., Bunkei, M., Moses, W., Nguyễn, H., Lehmann, M. K., O'Donnell, D., Ondrusek,
777 M., Han, T. H., Fichot, C. G., Moore, T. and Boss, E.: Robust algorithm for estimating total suspended
778 solids (TSS) in inland and nearshore coastal waters, *Remote Sens. Environ.*, 246(February), 111768,
779 doi:10.1016/j.rse.2020.111768, 2020.
- 780 Bhardwaj, J., Gupta, K. K. and Gupta, R.: A review of emerging trends on water quality measurement
781 sensors, *Proc. - Int. Conf. Technol. Sustain. Dev. ICTSD 2015*, (April), 1–6,
782 doi:10.1109/ICTSD.2015.7095919, 2015.
- 783 Bilotta, G. S. and Brazier, R. E.: Understanding the influence of suspended solids on water quality and
784 aquatic biota, *Water Res.*, 42(12), 2849–2861, doi:10.1016/j.watres.2008.03.018, 2008.
- 785 Bong, C. H. J. and Richard, J.: Drought and climate change assessment using standardized
786 precipitation index (Spi) for sarawak river basin, *J. Water Clim. Chang.*, 11(4), 956–965,
787 doi:10.2166/wcc.2019.036, 2020.
- 788 Brezonik, P. L., Olmanson, L. G., Finlay, J. C. and Bauer, M. E.: Factors affecting the measurement of
789 CDOM by remote sensing of optically complex inland waters, *Remote Sens. Environ.*, 157, 199–215,

790 doi:10.1016/j.rse.2014.04.033, 2015.

791 Cao, F., Tzortziou, M., Hu, C., Mannino, A., Fichot, C. G., Del Vecchio, R., Najjar, R. G. and Novak, M.:
792 Remote sensing retrievals of colored dissolved organic matter and dissolved organic carbon
793 dynamics in North American estuaries and their margins, *Remote Sens. Environ.*, 205(November
794 2017), 151–165, doi:10.1016/j.rse.2017.11.014, 2018.

795 Chapman, P. M., Hayward, A. and Faithful, J.: Total Suspended Solids Effects on Freshwater Lake
796 Biota Other than Fish, *Bull. Environ. Contam. Toxicol.*, 99(4), 423–427, doi:10.1007/s00128-017-
797 2154-y, 2017.

798 Chen, S., Huang, W., Chen, W. and Chen, X.: An enhanced MODIS remote sensing model for
799 detecting rainfall effects on sediment plume in the coastal waters of Apalachicola Bay, *Mar. Environ.
800 Res.*, 72(5), 265–272, doi:10.1016/j.marenvres.2011.09.014, 2011.

801 Chen, S., Han, L., Chen, X., Li, D., Sun, L. and Li, Y.: Estimating wide range Total Suspended Solids
802 concentrations from MODIS 250-m imageries: An improved method, *ISPRS J. Photogramm. Remote
803 Sens.*, 99, 58–69, doi:10.1016/j.isprsjprs.2014.10.006, 2015a.

804 Chen, S., Han, L., Chen, X., Li, D., Sun, L. and Li, Y.: Estimating wide range Total Suspended Solids
805 concentrations from MODIS 250-m imageries: An improved method, *ISPRS J. Photogramm. Remote
806 Sens.*, 99, 58–69, doi:10.1016/j.isprsjprs.2014.10.006, 2015b.

807 Chen, Z., Hu, C. and Muller-karger, F.: Monitoring turbidity in Tampa Bay using MODIS / Aqua 250-m
808 imagery, , 109, 207–220, doi:10.1016/j.rse.2006.12.019, 2007.

809 Cherukuru, N., Ford, P. W., Matear, R. J., Oubelkheir, K., Clementson, L. A., Suber, K. and Steven, A.
810 D. L.: Estimating dissolved organic carbon concentration in turbid coastal waters using optical
811 remote sensing observations, *Int. J. Appl. Earth Obs. Geoinf.*, 52, 149–154,
812 doi:10.1016/j.jag.2016.06.010, 2016a.

813 Cherukuru, N., Ford, P. W., Matear, R. J., Oubelkheir, K., Clementson, L. A., Suber, K. and Steven, A.
814 D. L.: Estimating dissolved organic carbon concentration in turbid coastal waters using optical
815 remote sensing observations, *Int. J. Appl. Earth Obs. Geoinf.*, 52, 149–154,
816 doi:10.1016/j.jag.2016.06.010, 2016b.

817 Cherukuru, N., Martin, P., Sanwani, N., Mujahid, A. and Müller, M.: A semi-analytical optical remote
818 sensing model to estimate suspended sediment and dissolved organic carbon in tropical coastal
819 waters influenced by peatland-draining river discharges off sarawak, borneo, *Remote Sens.*, 13(1), 1–
820 31, doi:10.3390/rs13010099, 2021.

821 Chong, X. Y., Gibbins, C. N., Vericat, D., Batalla, R. J., Teo, F. Y. and Lee, K. S. P.: A framework for
822 Hydrological characterisation to support Functional Flows (HyFFlow): Application to a tropical river,
823 *J. Hydrol. Reg. Stud.*, 36(January), doi:10.1016/j.ejrh.2021.100838, 2021.

824 CIFOR: Forest Carbon Database, [online] Available from: <https://carbonstock.cifor.org/>, n.d.

825 Cui, T., Zhang, J., Groom, S., Sun, L., Smyth, T. and Sathyendranath, S.: Remote Sensing of
826 Environment Validation of MERIS ocean-color products in the Bohai Sea : A case study for turbid
827 coastal waters, *Remote Sens. Environ.*, 114(10), 2326–2336, doi:10.1016/j.rse.2010.05.009, 2010.

828 Davies, J., Mathew, U., Aikanathan, S., Nyon, Y. C. and Chong, G.: A Quick Scan of Peatlands, *Wetl.
829 Int. Malaysia*, 1(March), 1–80, 2010.

830 Department of Environment: Malaysia Marine Water Quality Standards and Index, , 16 [online]
831 Available from: <https://www.doe.gov.my/portalv1/wp-content/uploads/2019/04/BOOKLET-BI.pdf>
832 (Accessed 12 September 2021), 2019.

833 Department of Statistics, M.: Sarawak Population, Popul. by Adm. Dist. Ethn. group, Sarawak, 2020
834 [online] Available from: https://sarawak.gov.my/web/home/article_view/240/175, 2020.

835 DID: Department of Irrigation & Drainage Sarawak: Introduction to Integrated Coastal Zone
836 Management, [online] Available from: [https://did.sarawak.gov.my/page-0-123-476-INTEGRATED-](https://did.sarawak.gov.my/page-0-123-476-INTEGRATED-COASTAL-ZONE-MANAGEMENT.html)
837 [COASTAL-ZONE-MANAGEMENT.html](https://did.sarawak.gov.my/page-0-123-476-INTEGRATED-COASTAL-ZONE-MANAGEMENT.html) (Accessed 21 October 2021a), 2021.

838 DID: Department Of Irrigation & Drainage Sarawak, 2021b.

839 Dindang, A., Chung, C. N. and Seth, S.: Heavy Rainfall Episodes over Sarawak during January-February
840 2011 Northeast Monsoon, *JMM Res. Publ.*, (11), 41, 2011.

841 Dogliotti, A. I., Ruddick, K. G., Nechad, B., Doxaran, D. and Knaeps, E.: A single algorithm to retrieve
842 turbidity from remotely-sensed data in all coastal and estuarine waters, *Remote Sens. Environ.*, 156,
843 157–168, doi:10.1016/j.rse.2014.09.020, 2015.

844 Donohue, I. and Garcia Molinos, J.: Impacts of increased sediment loads on the ecology of lakes, *Biol.*
845 *Rev.*, 84(4), 517–531, doi:10.1111/j.1469-185X.2009.00081.x, 2009.

846 Dorji, P. and Fearn, P.: Impact of the spatial resolution of satellite remote sensing sensors in the
847 quantification of total suspended sediment concentration: A case study in turbid waters of Northern
848 Western Australia, *PLoS One*, 12(4), 1–24, doi:10.1371/journal.pone.0175042, 2017.

849 Erftemeijer, P. L. A., Riegl, B., Hoeksema, B. W. and Todd, P. A.: Environmental impacts of dredging
850 and other sediment disturbances on corals: A review, *Mar. Pollut. Bull.*, 64(9), 1737–1765,
851 doi:10.1016/j.marpolbul.2012.05.008, 2012.

852 Espinoza Villar, R., Martinez, J. M., Le Texier, M., Guyot, J. L., Fraizy, P., Meneses, P. R. and Oliveira,
853 E. de: A study of sediment transport in the Madeira River, Brazil, using MODIS remote-sensing
854 images, *J. South Am. Earth Sci.*, 44, 45–54, doi:10.1016/j.jsames.2012.11.006, 2013.

855 European Space Agency: Sentinel-2, [online] Available from:
856 <https://sentinels.copernicus.eu/web/sentinel/user-guides/sentinel-2-msi/> (Accessed 29 October
857 2022a), 2022.

858 European Space Agency: Sentinel-3, [online] Available from:
859 <https://sentinel.esa.int/web/sentinel/missions/sentinel-3> (Accessed 29 October 2022b), 2022.

860 Fabricius, K. E.: Effects of terrestrial runoff on the ecology of corals and coral reefs: Review and
861 synthesis, *Mar. Pollut. Bull.*, 50(2), 125–146, doi:10.1016/j.marpolbul.2004.11.028, 2005.

862 Fabricius, K. E., Logan, M., Weeks, S. J., Lewis, S. E. and Brodie, J.: Changes in water clarity in
863 response to river discharges on the Great Barrier Reef continental shelf: 2002–2013, *Estuar. Coast.*
864 *Shelf Sci.*, 173, A1–A15, doi:10.1016/j.ecss.2016.03.001, 2016.

865 Gaveau, D. L. A., Sheil, D., Salim, M. A., Arjasakusuma, S., Ancrenaz, M., Pacheco, P. and Meijaard, E.:
866 Rapid conversions and avoided deforestation : examining four decades of industrial plantation
867 expansion in Borneo, *Nat. Publ. Gr.*, (September), 1–13, doi:10.1038/srep32017, 2016.

868 Gilmour, J. P., Cooper, T. F., Fabricius, K. E. and Smith, L. D.: Early warning indicators of change in the
869 condition of corals and coral communities in response to key anthropogenic stressors in the Pilbara,
870 Western Australia, *Aust. Inst. Mar. Sci. Rep. to Environ. Prot. Authority*. 101pp, 2006.

871 Giuliani, G., Chatenoux, B., Piller, T., Moser, F. and Lacroix, P.: Data Cube on Demand (DCoD):
872 Generating an earth observation Data Cube anywhere in the world, *Int. J. Appl. Earth Obs. Geoinf.*,
873 87(December 2019), 102035, doi:10.1016/j.jag.2019.102035, 2020.

874 Gomes, V. C. F., Carlos, F. M., Queiroz, G. R., Ferreira, K. R. and Santos, R.: Accessing and Processing

875 Brazilian Earth Observation Data Cubes With the Open Data Cube Platform, *ISPRS Ann. Photogramm.*
876 *Remote Sens. Spat. Inf. Sci.*, V-4–2021, 153–159, doi:10.5194/isprs-annals-v-4-2021-153-2021, 2021.

877 Gomyo, M. and Koichiro, K.: Spatial and temporal variations in rainfall and the ENSO-rainfall
878 relationship over Sarawak, Malaysian Borneo, *Sci. Online Lett. Atmos.*, 5, 41–44,
879 doi:10.2151/sola.2009-011, 2009.

880 González Vilas, L., Spyrakos, E. and Torres Palenzuela, J. M.: Neural network estimation of
881 chlorophyll a from MERIS full resolution data for the coastal waters of Galician rias (NW Spain),
882 *Remote Sens. Environ.*, 115(2), 524–535, doi:10.1016/j.rse.2010.09.021, 2011.

883 Ha, N. T. T., Thao, N. T. P., Koike, K. and Nhuan, M. T.: Selecting the best band ratio to estimate
884 chlorophyll-a concentration in a tropical freshwater lake using sentinel 2A images from a case study
885 of Lake Ba Be (Northern Vietnam), *ISPRS Int. J. Geo-Information*, 6(9), doi:10.3390/ijgi6090290,
886 2017.

887 Henley, W. F., Patterson, M. A., Neves, R. J. and Dennis Lemly, A.: Effects of Sedimentation and
888 Turbidity on Lotic Food Webs: A Concise Review for Natural Resource Managers, *Rev. Fish. Sci.*, 8(2),
889 125–139, doi:10.1080/10641260091129198, 2000.

890 Hodgson, G.: Tetracycline reduces sedimentation damage to corals, *Mar. Biol.*, 104(3), 493–496,
891 1990.

892 Hon, J. and Shibata, S.: A Review on Land Use in the Malaysian State of Sarawak, Borneo and
893 Recommendations for Wildlife Conservation Inside Production Forest Environment, *Borneo J.*
894 *Resour. Sci. Technol.*, 3(2), 22–35, doi:10.33736/bjrst.244.2013, 2013.

895 Horsburgh, J. S., Spackman, A., Stevens, D. K., Tarboton, D. G. and Mesner, N. O.: Environmental
896 Modelling & Software A sensor network for high frequency estimation of water quality constituent
897 fluxes using surrogates, , 25, 1031–1044, doi:10.1016/j.envsoft.2009.10.012, 2010.

898 Howarth, R. W.: Coastal nitrogen pollution: A review of sources and trends globally and regionally,
899 *Harmful Algae*, 8(1), 14–20, doi:10.1016/j.hal.2008.08.015, 2008.

900 Hu, C., Lee, Z. and Franz, B.: Chlorophyll a algorithms for oligotrophic oceans: A novel approach
901 based on three-band reflectance difference, *J. Geophys. Res. Ocean.*, 117(1), 1–25,
902 doi:10.1029/2011JC007395, 2012.

903 Jiang, D., Matsushita, B., Pahlevan, N., Gurlin, D., Lehmann, M. K., Fichot, C. G., Schalles, J., Loisel, H.,
904 Binding, C., Zhang, Y., Alikas, K., Kangro, K., Uusõue, M., Ondrusek, M., Greb, S., Moses, W. J.,
905 Lohrenz, S. and O'Donnell, D.: Remotely estimating total suspended solids concentration in clear to
906 extremely turbid waters using a novel semi-analytical method, *Remote Sens. Environ.*, 258,
907 doi:10.1016/j.rse.2021.112386, 2021.

908 Jiang, H. and Liu, Y.: Monitoring of TSS concentration in Poyang Lake based on MODIS data, *Yangtze*
909 *River*, 42(17), 87–90, 2011.

910 Kemp, P., Sear, D., Collins, A., Naden, P. and Jones, I.: The impacts of fine sediment on riverine fish,
911 *Hydrol. Process.*, 25(11), 1800–1821, doi:10.1002/hyp.7940, 2011.

912 Killough, B.: The Impact of Analysis Ready Data in the Africa Regional Data Cube, *Int. Geosci. Remote*
913 *Sens. Symp.*, (July 2019), 5646–5649, doi:10.1109/IGARSS.2019.8898321, 2019.

914 Kim, H. C., Son, S., Kim, Y. H., Khim, J. S., Nam, J., Chang, W. K., Lee, J. H., Lee, C. H. and Ryu, J.:
915 Remote sensing and water quality indicators in the Korean West coast: Spatio-temporal structures of
916 MODIS-derived chlorophyll-a and total suspended solids, *Mar. Pollut. Bull.*, 121(1–2), 425–434,
917 doi:10.1016/j.marpolbul.2017.05.026, 2017.

918 Krause, C., Dunn, B., Bishop-Taylor, R., Adams, C., Burton, C., Alger, M., Chua, S., Phillips, C., Newey,
919 V., Kouzoubov, K., Leith, A., Ayers, D., Hicks, A. and DEA Notebooks contributors 2021: Digital Earth
920 Australia notebooks and tools repository, , doi:<https://doi.org/10.26186/145234>, 2021.

921 Kuok, K. K., Chiu, P., Yap, A. and Law, K.: Determination of the Best Tank Model for the Southern
922 Region of Sarawak Determination Number of Tanks for Tank Model at Southern Region of Sarawak, ,
923 (August 2012), 2018.

924 Langer, O. E.: Effects of sedimentation on salmonid stream life, Environmental Protection Service.,
925 1980.

926 Lavigne, H., Van der Zande, D., Ruddick, K., Cardoso Dos Santos, J. F., Gohin, F., Brotas, V. and
927 Kratzer, S.: Quality-control tests for OC4, OC5 and NIR-red satellite chlorophyll-a algorithms applied
928 to coastal waters, *Remote Sens. Environ.*, 255, 112237, doi:[10.1016/j.rse.2020.112237](https://doi.org/10.1016/j.rse.2020.112237), 2021.

929 Lee, K. H., Noh, J. and Khim, J. S.: The Blue Economy and the United Nations' sustainable
930 development goals: Challenges and opportunities, *Environ. Int.*, 137(October 2019), 105528,
931 doi:[10.1016/j.envint.2020.105528](https://doi.org/10.1016/j.envint.2020.105528), 2020a.

932 Lee, W. C., Viswanathan, K. K., Kamri, T. and King, S.: Status of Sarawak Fisheries: Challenges and
933 Way Forward, *Int. J. Serv. Manag. Sustain.*, 5(2), 187–200, doi:[10.24191/ijms.v5i2.11719](https://doi.org/10.24191/ijms.v5i2.11719), 2020b.

934 Lehner, B., Verdin, K. and Jarvis, A.: HydroSHEDS technical documentation, World Wildl. Fund US,
935 Washington, DC, 1–27, 2006.

936 Lemley, D. A., Adams, J. B., Bornman, T. G., Campbell, E. E. and Deyzel, S. H. P.: Land-derived
937 inorganic nutrient loading to coastal waters and potential implications for nearshore plankton
938 dynamics, *Cont. Shelf Res.*, 174(August 2018), 1–11, doi:[10.1016/j.csr.2019.01.003](https://doi.org/10.1016/j.csr.2019.01.003), 2019.

939 Lewis, A., Oliver, S., Lymburner, L., Evans, B., Wyborn, L., Mueller, N., Raevksi, G., Hooke, J.,
940 Woodcock, R., Sixsmith, J., Wu, W., Tan, P., Li, F., Killough, B., Minchin, S., Roberts, D., Ayers, D.,
941 Bala, B., Dwyer, J., Dekker, A., Dhu, T., Hicks, A., Ip, A., Purss, M., Richards, C., Sagar, S., Trenham, C.,
942 Wang, P. and Wang, L. W.: The Australian Geoscience Data Cube — Foundations and lessons
943 learned, *Remote Sens. Environ.*, 202, 276–292, doi:[10.1016/j.rse.2017.03.015](https://doi.org/10.1016/j.rse.2017.03.015), 2017.

944 Limcih, F., Jilnm, M., Hb, H., Ilcach, H. N. M., Mnl, F., Fi, F. and Nb, F.: Study of Coastal Areas in Miri,
945 in *World Engineering Congress 2010*, pp. 56–65., 2010.

946 Ling, T. Y., Soo, C. L., Sivalingam, J. R., Nyanti, L., Sim, S. F. and Grinang, J.: Assessment of the Water
947 and Sediment Quality of Tropical Forest Streams in Upper Reaches of the Baleh River, Sarawak,
948 Malaysia, Subjected to Logging Activities, *J. Chem.*, 2016, doi:[10.1155/2016/8503931](https://doi.org/10.1155/2016/8503931), 2016.

949 Liu, B., D'Sa, E. J. and Joshi, I.: Multi-decadal trends and influences on dissolved organic carbon
950 distribution in the Barataria Basin, Louisiana from in-situ and Landsat/MODIS observations, *Remote
951 Sens. Environ.*, 228(May), 183–202, doi:[10.1016/j.rse.2019.04.023](https://doi.org/10.1016/j.rse.2019.04.023), 2019.

952 Loisel, H., Mangin, A., Vantrepotte, V., Dessailly, D., Ngoc Dinh, D., Garnesson, P., Ouilon, S.,
953 Lefebvre, J. P., Mériaux, X. and Minh Phan, T.: Variability of suspended particulate matter
954 concentration in coastal waters under the Mekong's influence from ocean color (MERIS) remote
955 sensing over the last decade, *Remote Sens. Environ.*, 150, 218–230, doi:[10.1016/j.rse.2014.05.006](https://doi.org/10.1016/j.rse.2014.05.006),
956 2014.

957 Long, S. M.: Sarawak Coastal Biodiversity : A Current Status, *Kuroshio Sci.*, 8(1), 71–84 [online]
958 Available from: <https://www.researchgate.net/publication/265793245>, 2014.

959 Lu, Y., Yuan, J., Lu, X., Su, C., Zhang, Y., Wang, C., Cao, X., Li, Q., Su, J., Ittekkot, V., Garbutt, R. A.,
960 Bush, S., Fletcher, S., Wagey, T., Kachur, A. and Sweijid, N.: Major threats of pollution and climate

961 change to global coastal ecosystems and enhanced management for sustainability, *Environ. Pollut.*,
962 239, 670–680, doi:10.1016/j.envpol.2018.04.016, 2018.

963 Macklin, M. G., Jones, A. F. and Lewin, J.: River response to rapid Holocene environmental change:
964 evidence and explanation in British catchments, *Quat. Sci. Rev.*, 29(13–14), 1555–1576,
965 doi:10.1016/j.quascirev.2009.06.010, 2010.

966 Mao, Z., Chen, J., Pan, D., Tao, B. and Zhu, Q.: A regional remote sensing algorithm for total
967 suspended matter in the East China Sea, *Remote Sens. Environ.*, 124, 819–831,
968 doi:10.1016/j.rse.2012.06.014, 2012.

969 Martin, P., Cherukuru, N., Tan, A. S. Y., Sanwlan, N., Mujahid, A. and Müller, M.: Distribution and
970 cycling of terrigenous dissolved organic carbon in peatland-draining rivers and coastal waters of
971 Sarawak, Borneo, *Biogeosciences*, 15(22), 6847–6865, doi:10.5194/bg-15-6847-2018, 2018.

972 Mengen, D., Ottinger, M., Leinenkugel, P. and Ribbe, L.: Modeling river discharge using automated
973 river width measurements derived from sentinel-1 time series, *Remote Sens.*, 12(19), 1–24,
974 doi:10.3390/rs12193236, 2020.

975 Milliman, J. D. and Farnsworth, K. L.: *River discharge to the coastal ocean: a global synthesis*,
976 Cambridge University Press., 2013.

977 Mohammad Razi, M. A., Mokhtar, A., Mahamud, M., Rahmat, S. N. and Al-Gheethi, A.: Monitoring of
978 river and marine water quality at Sarawak baseline, *Environ. Forensics*, 22(1–2), 219–240,
979 doi:10.1080/15275922.2020.1836076, 2021.

980 Morel, A. and Bélanger, S.: Improved detection of turbid waters from ocean color sensors
981 information, *Remote Sens. Environ.*, 102(3–4), 237–249, doi:10.1016/j.rse.2006.01.022, 2006.

982 Morel, A. and Gentili, B.: A simple band ratio technique to quantify the colored dissolved and detrital
983 organic material from ocean color remotely sensed data, *Remote Sens. Environ.*, 113(5), 998–1011,
984 doi:10.1016/j.rse.2009.01.008, 2009.

985 Mueller, J., Mueller, J., Pietras, C., Hooker, S., Clark, D., Frouin, A., Mitchell, B., Bidigare, R., Trees, C.
986 and Werdell, J.: *Ocean Optics Protocols For Satellite Ocean Color Sensor Validation, Revision 3*,
987 volumes 1 and 2., 2002.

988 Müller-dum, D., Warneke, T., Rixen, T., Müller, M., Baum, A., Christodoulou, A., Oakes, J., Eyre, B. D.
989 and Notholt, J.: Impact of peatlands on carbon dioxide (CO₂) emissions from the Rajang River and
990 Estuary, Malaysia, , 17–32, 2019.

991 Müller, D., Warneke, T., Rixen, T., Müller, M., Mujahid, A., Bange, H. W. and Notholt, J.: Fate of
992 terrestrial organic carbon and associated CO₂ and CO emissions from two Southeast Asian estuaries,
993 *Biogeosciences*, 13(3), 691–705, doi:10.5194/bg-13-691-2016, 2016.

994 NASA official: Spectral Characterization Data by Sensor, [online] Available from:
995 https://oceancolor.gsfc.nasa.gov/docs/rsr/rsr_tables/#MODIS-AQUA (Accessed 29 October 2022),
996 2022.

997 NASA Official: Ocean Level-2 Data Format Specification, [online] Available from:
998 <https://oceancolor.gsfc.nasa.gov/docs/format/l2nc/>, n.d.

999 Nazirova, K., Alferyeva, Y., Lavrova, O., Shur, Y., Soloviev, D., Bocharova, T. and Stochkov, A.:
1000 Comparison of in situ and remote-sensing methods to determine turbidity and concentration of
1001 suspended matter in the estuary zone of the mzymta river, black sea, *Remote Sens.*, 13(1), 1–29,
1002 doi:10.3390/rs13010143, 2021.

1003 Neil, C., Spyarakos, E., Hunter, P. D. and Tyler, A. N.: A global approach for chlorophyll-a retrieval

1004 across optically complex inland waters based on optical water types, *Remote Sens. Environ.*,
1005 229(May), 159–178, doi:10.1016/j.rse.2019.04.027, 2019.

1006 Ondrusek, M., Stengel, E., Kinkade, C. S., Vogel, R. L., Keegstra, P., Hunter, C. and Kim, C.: The
1007 development of a new optical total suspended matter algorithm for the Chesapeake Bay, *Remote*
1008 *Sens. Environ.*, 119, 243–254, doi:10.1016/j.rse.2011.12.018, 2012.

1009 Open Data Cube: Open Data Cube, [online] Available from:
1010 <https://opendatacube.readthedocs.io/en/latest/user/intro.html> (Accessed 25 October 2021), 2021.

1011 Pahlevan, N., Smith, B., Binding, C. and O'Donnell, D. M.: Spectral band adjustments for remote
1012 sensing reflectance spectra in coastal/inland waters, , 25(23), 2574–2591 [online] Available from:
1013 <http://arxiv.org/abs/1207.0580>, 2012.

1014 Park, G. S.: The role and distribution of total suspended solids in the macrotidal coastal waters of
1015 Korea, *Environ. Monit. Assess.*, 135(1–3), 153–162, doi:10.1007/s10661-007-9640-3, 2007.

1016 Petus, C., Marieu, V., Novoa, S., Chust, G., Bruneau, N. and Froidefond, J. M.: Monitoring spatio-
1017 temporal variability of the Adour River turbid plume (Bay of Biscay, France) with MODIS 250-m
1018 imagery, *Cont. Shelf Res.*, 74, 35–49, doi:10.1016/j.csr.2013.11.011, 2014.

1019 Praveena, S. M., Siraj, S. S. and Aris, A. Z.: Coral reefs studies and threats in Malaysia: A mini review,
1020 *Rev. Environ. Sci. Biotechnol.*, 11(1), 27–39, doi:10.1007/s11157-011-9261-8, 2012.

1021 Ramaswamy, V., Rao, P. S., Rao, K. H., Thwin, S., Rao, N. S. and Raiker, V.: Tidal influence on
1022 suspended sediment distribution and dispersal in the northern Andaman Sea and Gulf of Martaban,
1023 *Mar. Geol.*, 208(1), 33–42, doi:10.1016/j.margeo.2004.04.019, 2004.

1024 Refaeilzadeh, P., Tang, L., Liu, H., Angeles, L. and Scientist, C. D.: *Encyclopedia of Database Systems*,
1025 *Encycl. Database Syst.*, doi:10.1007/978-1-4899-7993-3, 2020.

1026 Risk, M. J. and Edinger, E.: Impacts of sediment on coral reefs, *Encycl. Mod. coral reefs*. Springer,
1027 Netherlands, 575–586, 2011.

1028 Rogers, C. S.: The effect of shading on coral reef structure and function, *J. Exp. Mar. Bio. Ecol.*, 41(3),
1029 269–288, doi:10.1016/0022-0981(79)90136-9, 1979.

1030 Sa'adi, Z., Shahid, S., Chung, E. S. and Ismail, T. bin: Projection of spatial and temporal changes of
1031 rainfall in Sarawak of Borneo Island using statistical downscaling of CMIP5 models, *Atmos. Res.*,
1032 197(November 2016), 446–460, doi:10.1016/j.atmosres.2017.08.002, 2017.

1033 Sandifer, P. A., Keener, P., Scott, G. I. and Porter, D. E.: *Oceans and Human Health and the New Blue*
1034 *Economy*, Elsevier Inc., 2021.

1035 Sarawak Forestry Corporation: Maludam National Park, [online] Available from:
1036 <https://sarawakforestry.com/parks-and-reserves/maludam-national-park/>, 2022.

1037 Seegers, B. N., Stumpf, R. P., Schaeffer, B. A., Loftin, K. A. and Werdell, P. J.: Performance metrics for
1038 the assessment of satellite data products: an ocean color case study, *Opt. Express*, 26(6), 7404,
1039 doi:10.1364/oe.26.007404, 2018.

1040 Shaw, E. Al and Richardson, J. S.: Direct and indirect effects of sediment pulse duration on stream
1041 invertebrate assemblages and rainbow trout (*Oncorhynchus mykiss*) growth and survival, *Can. J.*
1042 *Fish. Aquat. Sci.*, 58(11), 2213–2221, doi:10.1139/f01-160, 2001.

1043 Sim, C., Cherukuru, N., Mujahid, A., Martin, P., Sanwlani, N., Warneke, T., Rixen, T., Notholt, J. and
1044 Müller, M.: A new remote sensing method to estimate river to ocean DOC flux in peatland
1045 dominated Sarawak coastal regions, Borneo, *Remote Sens.*, 12(20), 1–13, doi:10.3390/rs12203380,

- 1046 2020.
- 1047 Siswanto, E., Tang, J. and Yamaguchi, H.: Empirical ocean-color algorithms to retrieve chlorophyll- a,
1048 total suspended matter , and colored dissolved organic matter absorption coefficient in the Yellow
1049 and East China Seas, , 627–650, doi:10.1007/s10872-011-0062-z, 2011.
- 1050 Slonecker, E. T., Jones, D. K. and Pellerin, B. A.: The new Landsat 8 potential for remote sensing of
1051 colored dissolved organic matter (CDOM), *Mar. Pollut. Bull.*, 107(2), 518–527,
1052 doi:10.1016/j.marpolbul.2016.02.076, 2016.
- 1053 Song, C., Wang, G., Sun, X., Chang, R. and Mao, T.: Control factors and scale analysis of annual river
1054 water, sediments and carbon transport in China, *Sci. Rep.*, 6(May), 1–14, doi:10.1038/srep25963,
1055 2016.
- 1056 Song, Z., Shi, W., Zhang, J., Hu, H., Zhang, F. and Xu, X.: Transport mechanism of suspended
1057 sediments and migration trends of sediments in the central hangzhou bay, *Water (Switzerland)*,
1058 12(8), doi:10.3390/W12082189, 2020.
- 1059 Soo, C. L., Chen, C. A. and Mohd-Long, S.: Assessment of Near-Bottom Water Quality of
1060 Southwestern Coast of Sarawak, Borneo, Malaysia: A Multivariate Statistical Approach, *J. Chem.*,
1061 2017, doi:10.1155/2017/1590329, 2017.
- 1062 Soum, S., Ngor, P. B., Dilts, T. E., Lohani, S., Kelson, S., Null, S. E., Tromboni, F., Hogan, Z. S., Chan, B.
1063 and Chandra, S.: Spatial and long-term temporal changes in water quality dynamics of the tonle sap
1064 ecosystem, *Water (Switzerland)*, 13(15), doi:10.3390/w13152059, 2021.
- 1065 Staub, J. R. and Esterle, J. S.: Provenance and sediment dispersal in the Rajang River delta/coastal
1066 plain system, Sarawak, East Malaysia, *Sediment. Geol.*, 85(1–4), 191–201, doi:10.1016/0037-
1067 0738(93)90083-H, 1993.
- 1068 Staub, J. R., Among, H. L. and Gastaldo, R. A.: Seasonal sediment transport and deposition in the
1069 Rajang River delta, Sarawak, East Malaysia, *Sediment. Geol.*, 133(3–4), 249–264, doi:10.1016/S0037-
1070 0738(00)00042-7, 2000.
- 1071 Sun, C.: Riverine influence on ocean color in the equatorial South China Sea, *Cont. Shelf Res.*,
1072 143(December 2015), 151–158, doi:10.1016/j.csr.2016.10.008, 2017a.
- 1073 Sun, C.: Riverine influence on ocean color in the equatorial South China Sea, *Cont. Shelf Res.*,
1074 143(October 2016), 151–158, doi:10.1016/j.csr.2016.10.008, 2017b.
- 1075 Sutherland, A. B. and Meyer, J. L.: Effects of increased suspended sediment on growth rate and gill
1076 condition of two southern Appalachian minnows, *Environ. Biol. Fishes*, 80(4), 389–403,
1077 doi:10.1007/s10641-006-9139-8, 2007.
- 1078 Swain, R. and Sahoo, B.: Mapping of heavy metal pollution in river water at daily time-scale using
1079 spatio-temporal fusion of MODIS-aqua and Landsat satellite imageries, *J. Environ. Manage.*, 192, 1–
1080 14, doi:10.1016/j.jenvman.2017.01.034, 2017.
- 1081 Tangang, F. T., Juneng, L., Salimun, E., Sei, K. M., Le, L. J. and Muhamad, H.: Climate change and
1082 variability over Malaysia: Gaps in science and research information, *Sains Malaysiana*, 41(11), 1355–
1083 1366, 2012.
- 1084 Tawan, A. S., Ling, T. Y., Nyanti, L., Sim, S. F., Grinang, J., Soo, C. L., Lee, K. S. P. and Ganyai, T.:
1085 Assessment of water quality and pollutant loading of the Rajang River and its tributaries at Pelagus
1086 area subjected to seasonal variation and river regulation, *Environ. Dev. Sustain.*, 22(5), 4101–4124,
1087 doi:10.1007/s10668-019-00374-9, 2020.
- 1088 Telesnicki, G. J. and Goldberg, W. M.: CORAL REEF PAPER EFFECTS OF TURBIDITY ON THE

1089 PHOTOSYNTHESIS AND RESPIRATION OF TWO SOUTH FLORIDA REEF CORAL SPECIES portant factors
1090 in the regulation of coral cover , diversity , and abundance (Ed- ships between suspended sediment
1091 concentrations or parti , , 57(2), 527–539, 1995.

1092 Tromboni, F., Dilts, T. E., Null, S. E., Lohani, S., Ngor, P. B., Soum, S., Hogan, Z. and Chandra, S.:
1093 Changing land use and population density are degrading water quality in the lower mekong basin,
1094 Water (Switzerland), 13(14), 1–16, doi:10.3390/w13141948, 2021.

1095 United Nations: The Ocean Conference, in The Ocean Conference, vol. 53, p. 130, New York., 2017.

1096 Valerio, A. de M., Kampel, M., Vantrepotte, V., Ward, N. D., Sawakuchi, H. O., Less, D. F. D. S., Neu,
1097 V., Cunha, A. and Richey, J.: Using CDOM optical properties for estimating DOC concentrations and
1098 pCO₂ in the Lower Amazon River , Opt. Express, 26(14), A657, doi:10.1364/oe.26.00a657, 2018.

1099 Verschelling, E., van der Deijl, E., van der Perk, M., Sloff, K. and Middelkoop, H.: Effects of discharge,
1100 wind, and tide on sedimentation in a recently restored tidal freshwater wetland, Hydrol. Process.,
1101 31(16), 2827–2841, doi:10.1002/hyp.11217, 2017.

1102 Vijith, H., Hurmain, A. and Dodge-Wan, D.: Impacts of land use changes and land cover alteration on
1103 soil erosion rates and vulnerability of tropical mountain ranges in Borneo, Remote Sens. Appl. Soc.
1104 Environ., 12(September), 57–69, doi:10.1016/j.rsase.2018.09.003, 2018.

1105 Wang, C., Chen, S., Li, D., Wang, D., Liu, W. and Yang, J.: A Landsat-based model for retrieving total
1106 suspended solids concentration of estuaries and coasts in China, Geosci. Model Dev., 10(12), 4347–
1107 4365, doi:10.5194/gmd-10-4347-2017, 2017.

1108 Wang, J., Tong, Y., Feng, L., Zhao, D., Zheng, C. and Tang, J.: Satellite-Observed Decreases in Water
1109 Turbidity in the Pearl River Estuary: Potential Linkage With Sea-Level Rise, J. Geophys. Res. Ocean.,
1110 126(4), 1–17, doi:10.1029/2020JC016842, 2021.

1111 Weber, M., Lott, C. and Fabricius, K. E.: Sedimentation stress in a scleractinian coral exposed to
1112 terrestrial and marine sediments with contrasting physical, organic and geochemical properties, J.
1113 Exp. Mar. Bio. Ecol., 336(1), 18–32, doi:10.1016/j.jembe.2006.04.007, 2006.

1114 Werdell, P. J., McKinna, L. I. W., Boss, E., Ackleson, S. G., Craig, S. E., Gregg, W. W., Lee, Z.,
1115 Maritorena, S., Roesler, C. S., Rousseaux, C. S., Stramski, D., Sullivan, J. M., Twardowski, M. S.,
1116 Tzortziou, M. and Zhang, X.: An overview of approaches and challenges for retrieving marine
1117 inherent optical properties from ocean color remote sensing, Prog. Oceanogr., 160, 186–212,
1118 doi:10.1016/j.pocean.2018.01.001, 2018.

1119 Whitmore, T. C.: Tropical rain forests of the Par East, Oxford. Clarendon Press., 1984.

1120 Wilber, D. H. and Clarke, D. G.: Biological Effects of Suspended Sediments: A Review of Suspended
1121 Sediment Impacts on Fish and Shellfish with Relation to Dredging Activities in Estuaries, North Am. J.
1122 Fish. Manag., 21(4), 855–875, doi:10.1577/1548-8675(2001)021<0855:beossa>2.0.co;2, 2001.

1123 World Bank and United Nations Department of Economic and Social Affairs (UNDESA): The Potential
1124 of the Blue Economy: Increasing Long-term Benefits of the Sustainable Use of Marine Resources for
1125 Small Island Developing States and Coastal Least Developed Countries, World Bank, Washington DC.,
1126 2017.

1127 Wu, C. S., Yang, S. L. and Lei, Y. ping: Quantifying the anthropogenic and climatic impacts on water
1128 discharge and sediment load in the Pearl River (Zhujiang), China (1954–2009), J. Hydrol., 452–453,
1129 190–204, doi:10.1016/j.jhydrol.2012.05.064, 2012.

1130 Yang, S. L., Zhao, Q. Y. and Belkin, I. M.: Temporal variation in the sediment load of the Yangtze river
1131 and the influences of human activities, J. Hydrol., 263(1–4), 56–71, doi:10.1016/S0022-

1132 1694(02)00028-8, 2002.

1133 Zhan, W., Wu, J., Wei, X., Tang, S. and Zhan, H.: Spatio-temporal variation of the suspended
1134 sediment concentration in the Pearl River Estuary observed by MODIS during 2003–2015, *Cont. Shelf*
1135 *Res.*, 172(May 2018), 22–32, doi:10.1016/j.csr.2018.11.007, 2019.

1136 Zhang, L. J., Wang, L., Cai, W. J., Liu, D. M. and Yu, Z. G.: Impact of human activities on organic carbon
1137 transport in the Yellow River, *Biogeosciences*, 10(4), 2513–2524, doi:10.5194/bg-10-2513-2013,
1138 2013.

1139 Zhang, M., Tang, J., Dong, Q., Song, Q. T. and Ding, J.: Retrieval of total suspended matter
1140 concentration in the Yellow and East China Seas from MODIS imagery, *Remote Sens. Environ.*,
1141 114(2), 392–403, doi:10.1016/j.rse.2009.09.016, 2010a.

1142 Zhang, Y., Lin, S., Liu, J., Qian, X. and Ge, Y.: Time-series MODIS image-based retrieval and
1143 distribution analysis of total suspended matter concentrations in Lake Taihu (China), *Int. J. Environ.*
1144 *Res. Public Health*, 7(9), 3545–3560, doi:10.3390/ijerph7093545, 2010b.

1145 Zhou, Y., Xuan, J. and Huang, D.: Tidal variation of total suspended solids over the Yangtze Bank
1146 based on the geostationary ocean color imager, *Sci. China Earth Sci.*, 63(9), 1381–1389,
1147 doi:10.1007/s11430-019-9618-7, 2020.

1148

1149

1150

1151

1152

1153

1154

1155

1156

1157

1158

1159

1160

1161

1162

1163

1164